Cellulose-based Adsorbent of Animal Waste for the Adsorption of Lead and Phenol

Patrick T. Ngueagni,[a,*] Mohamed Hefnawy,[b] Edwin Andrew Ofudje,[c] Ali El Gamal,[d] James Asamu Akande,[e] and Talha Bin Emran [f,g]

The adsorption of phenol and Pb^{2+} from aqueous solutions was achieved using calcined animal waste (cow dung) as a low-cost adsorbent. Fourier transform infrared analysis confirmed the involvement of hydroxyl, carbonate, and possibly silicate functional groups in the adsorption process. Scanning electron microscope images revealed the presence of distinct rod-like fibers on the adsorbent surface. Adsorption kinetics revealed an increase in pollutant uptake over time, with the effect being more pronounced at a higher initial concentration of 280 mg/L. The optimal pH for maximum adsorption was identified as 6.5 for phenol and 4.5 for lead. Langmuir isotherm analysis indicated a higher adsorption affinity for lead, with a maximum adsorption capacity of 101 mg/g, compared to 89.3 mg/g for phenol. Conversely, the Freundlich isotherm model demonstrated a better fit for phenol adsorption. Thermodynamic evaluations showed negative $\Delta G°$ values, confirming the spontaneous nature of the sorption process for both pollutants. The enthalpy change ($\Delta H°$) values of 11.6 kJ/mol for phenol and 21.7 kJ/mol for lead validated the endothermic nature of the adsorption. These results underscore the effectiveness of calcined animal waste as a sustainable and efficient adsorbent for eliminating phenol and lead from wastewater.

DOI: 10.15376/biores.20.2.3923-3952

Keywords: Adsorbent; Adsorption; Animal waste; Cellulose; Contaminants

Contact information: a: Department of Inorganic Chemistry, Faculty of Science, University of Yaoundé, 812, Yaoundé, Cameroon; b: Department of Pharmaceutical Chemistry, College of Pharmacy, King Saud University, Riyadh 11451, Saudi Arabia; c: Department of Chemical Sciences, Mountain Top University, Ogun State, Nigeria; d: Department of Pharmacognosy, College of Pharmacy, King Saud University, Riyadh 11451, Saudi Arabia; e: Department of Chemistry and Biochemistry, Caleb University, Imota, Lagos State, Nigeria; f: Department of Pathology and Laboratory Medicine, Warren Alpert Medical School, Brown University, Providence, RI 02912, USA; g: Department of Pharmacy, Faculty of Health and Life Science, Daffodil International University, Dhaka 1207, Bangladesh;
** Corresponding author: patrickngueagn@gmail.com*

INTRODUCTION

Access to clean water is fundamental to the health and well-being of all living organisms on our planet. Water is also vital not only for human survival but also for the ecosystems that support diverse forms of life. Clean water facilitates essential functions, such as hydration, sanitation, agriculture, and various industrial processes, contributing to overall public health and environmental sustainability (Howard *et al*. 2016; Alshomali and Gulseven 2020). Without water in its best form, both humans and wildlife can suffer from dehydration, disease, and habitat destruction. Water sources, such as lakes and rivers in both developed and developing countries, have experienced significant contamination due to various human activities, including fertilizer production,

electroplating, leather tanning, sugar milling, textile manufacturing, mining, metallurgical processes, and municipal waste management (Akhtar *et al.* 2021). Industrial discharges often release heavy metals and toxic organic pollutants into water bodies, thereby severely impacting water quality (Babu and Prasanna 2019). The presence of these contaminants poses serious threats to aquatic ecosystems, terrestrial life, and human health, making their management and prevention a critical issue (Briffa *et al.* 2020).

Industrial wastewater effluents typically contain heavy metals in high concentrations, among which are lead, cadmium, arsenic, mercury, and chromium, alongside organic pollutants such as dyes (Issabayeva *et al*. 2017; Thilakan *et al*. 2022). Heavy metals present challenges due to their non-biodegradable nature, toxicity, carcinogenicity, and could lead to bioaccumulation within the food chain. Similarly, even low concentrations of organic pollutants in water can render it unsafe for human and animal consumption (Wang *et al*. 2020; Vesali-Naseh *et al*. 2021). Therefore, addressing the release of these harmful substances into water systems is of paramount importance.

Lead is found naturally within the Earth's crust as an element. Historically it has been used for a variety of industrial purposes. However, it is highly toxic. It affects human health and the environment even at low concentrations (Kucherova *et al*. 2017; Vesali-Naseh *et al*. 2021; Wang and Zhang 2021). Water contaminated with lead levels exceeding 0.07 mg/g poses health risks that can affect the brain, kidneys, and nervous system (Samira *et al.* 2022). Lead is a non-biodegradable metal that poses important risks to both human health and the environment. Its impact includes damage to the nervous system, leading to memory problems and impairments in children's behavior and cognitive development. Lead exposure is also related to an increased risk of cardiovascular diseases, such as coronary artery and hypertension disease. Additionally, it can cause gastrointestinal disturbances, nausea, manifesting as abdominal pain, and constipation, as well as respiratory issues, including coughing, difficulty breathing, and mucous membrane irritation. Furthermore, lead adversely affects reproductive health in both men and women, potentially resulting in fertility challenges (Ettinger *et al.* 2019; Aliyu and Musa 2021; Collina *et al.* 2022; Kshyanaprava and Alok 2023). Additionally, lead has the potential to impact various organs, including the liver, kidneys, and nervous system (Chen *et al*. 2019). The effects of lead are not limited to the biological environment alone; they also affect the physical environment through various means, such as industrial discharges, mining activities, and the use of lead in plumbing systems. All these factors contribute to water pollution, which could pose challenges for aquatic organisms (Aliyu and Musa 2021; Collina *et al.* 2022; Kshyanaprava, and Alok 2023). It has been noted that lead exposure can have toxic effects on plant roots, which may result in challenges to their growth and development and previous studies suggest that exposure to lead may lead to structural changes in plant cells, such as an increase in vacuolar volume and modifications in cell shape (Ettinger *et al.* 2019; Aliyu and Musa 2021).

Given its toxicity, addressing lead contamination in aquatic systems is crucial due to the potential health risks involved. It is important to ensure that lead is thoroughly monitored and appropriately removed from wastewater before disposal. In line with WHO guidelines, lead levels in wastewater and agricultural soils should remain below 0.01 and 0.1 ppm to safeguard public health and the environment (Kinuthia *et al*. 2020).

Certain industrial process effluents may contain phenol-based compounds, which could also potentially pose severe environmental risks. Phenols are known for their high solubility in water. Even at concentrations as low as 5 micrograms per liter (5 μg/L), they

can contribute to undesirable tastes and odors in water supplies (Sarker *et al*. 2017). Phenol-containing compounds may find their way into bodies of water because of various industrial activities, which include the pharmaceutical industry, tanning, textiles, the use of disinfectants, coal tar production, gasoline refining, plastics manufacturing, steel production, pesticide application, paint usage, domestic wastewater discharge, the paper industry, and the disposal of chemicals (Flouret *et al*. 2018; Hamdy *et al*. 2023). Exposure to phenol through the skin or respiratory tract can pose health risks, including potential poisoning. At higher concentrations, it may lead to protein precipitation, which can cause direct cellular damage, whereas at lower concentrations, phenol can induce protein denaturation (Shen *et al*. 2019). Because lead and phenol are recognized as significant pollutants in water systems, addressing their presence is essential for maintaining clean and healthy water.

Various approaches have been employed to effectively remove pollutants from water. They include filtration, flocculation/coagulation, precipitation, adsorption, chemical reduction, ion exchange, electrocoagulation, immobilization, bioremediation, and electro-kinetic remediation (Ofudje *et al*. 2020; Al-Ayed *et al*. 2022). However, many of these methods are costly and often ineffective in completely treating a wide range of pollutants.

Among these techniques, adsorption is widely regarded as a highly effective physicochemical method for pollutant removal from wastewater. It involves the transfer of a solute from the liquid phase onto the solid surface through physical or chemical interactions (Ofudje *et al*. 2014; Kanamarlapudi *et al*. 2018). Adsorption stands out due to its cost-effectiveness, simplicity, and the ability to regenerate adsorbents, making it a preferred choice for wastewater treatment (Adeogun *et al*. 2012; Ofudje *et al*. 2014). Despite these advantages, the challenge lies in developing adsorbents that are not only efficient but also safe and environmentally friendly (Nabipour *et al*. 2023). A couple of adsorbents have been explored for their potential to eliminate lead and phenol from wastewater. Examples include carbon nanoparticles impregnated on clay aggregate (Ghahremani *et al*. 2021), lignin-grafted carbon nanotubes (Li *et al*. 2017), Dijah-Monkin bentonite clay (Alexander *et al*. 2018), acid-treated pyrolytic tire char (Makrigianni *et al*. 2015), garlic peel (Muthamilselvi *et al*. 2016), corn husk activated carbon (Mishra *et al*. 2019), and pottery granules (Mohammad *et al*. 2023). These advancements highlight the ongoing efforts to improve the efficiency and ecological compatibility of adsorption technologies.

The adsorption of phenol onto multiwalled carbon nanotubes was investigated by Abdel-Ghani *et al*. (2015). Batch adsorption experiments were used to assess the removal efficiency of phenol under varying conditions, with equilibrium achieved within 300 minutes at an initial concentration of 25 mg/L, an optimal adsorbent dosage of 5 g/L, and a neutral pH of 7. The study underscores the efficacy of MWCNTs in adsorbing phenol, providing insights into adsorption kinetics and equilibrium behavior, which are crucial for optimizing treatment processes targeting phenolic contaminants. The adsorption capacity of phenol using activated carbon derived from lignocellulosic agriculture wastes of sugarcane bagasse and sawdust was explored by Haitham *et al*. (2022). Phenol maximum adsorption of 159 mg/g was achieved under optimal conditions, with adsorption following a pseudo-second-order kinetic model and fitting the Langmuir isotherm, highlighting the potential of waste-derived AC as an eco-friendly and cost-effective solution for phenol removal from water. Al-Ayed *et al*. (2022) explored the use of treated oil shale ash (OSA) as an adsorbent for lead (Pb^2) removal from water. The

results showed that adsorption capacity increased with pH, reaching optimal efficiency in slightly acidic to neutral conditions. Kinetic analysis revealed that adsorption followed a pseudo-second-order model, while equilibrium data fitted the Langmuir isotherm, indicating monolayer adsorption. The study on the kinetic of Pb(II) adsorption from aqueous medial onto carbon materials was examined by Kucherova *et al*. (2017). The study highlights the crucial role of surface functional groups in enhancing Pb^{2+} adsorption and demonstrates that equilibrium time, rate constants, and adsorption capacities vary among the tested materials.

Cellulosic materials that possess homogenous surfaces are among the most abundant natural resources available, offering a renewable and biodegradable option that is also cost-effective. The bio-based and biodegradable properties of cellulosic materials make them valuable for use as adsorbents. Their application and appropriate disposal can significantly aid in the enrichment and isolation of environmental pollutants; utilizing cellulosic animal waste as an adsorbent offers a promising solution for the removal of pollutants in wastewater (Thakur *et al*. 2020).

Animal waste, such as cow dung, is a form of lignocellulosic biomass. As such, it contains various components, including cellulose in its extensively crystallized form, hemicellulose, and lignin in its amorphous state, along with pectin, wax, and several additional substances (Puri *et al*. 2020; Qasim *et al*. 2021). Recent studies have indicated that biomass materials derived from cow dung exhibit favorable porous structures and an appealing specific surface area (Chen *et al*. 2022). A significant portion, around 90%, of cow dung remains unused as waste, primarily due to the limited availability of professional treatment facilities. Timely and proper management of this waste is crucial, as inadequate handling may potentially lead to environmental concerns, including water, soil, and air pollution (Wadekar *et al*. 2020). The benefits of using cow dung as an adsorbent extend beyond its low economic value; it also presents an opportunity to mitigate certain undesirable properties often associated with it. This study examined the potential of utilizing cellulose-based materials derived from animal waste (cow dung) for the adsorption of lead and phenol in industrial wastewater.

METHODOLOGY

Collection and Preparation of Animal Waste (AW)

Fresh cow dung was collected from a cow shed in Kara, a locality near Lagos, Nigeria, specifically at Kara Market along the Lagos-Ibadan Expressway in Ogun State (6.6516° N, 3.3470° E). The collected waste was air-dried for 48 to 72 hours to remove excess moisture. Once dried, it was placed in a muffle furnace and heated at 600 °C for 3 h. After calcination, the material was allowed to cool to room temperature in a desiccator to prevent moisture absorption. The cooled calcined waste was then ground into a fine powder using a mortar and pestle and labeled as calcined animal waste (CAW). Finally, the CAW was stored in an airtight container to prevent moisture uptake and contamination.

Characterization of Calcined Animal Waste (CAW)

The characterization of the adsorbent can be regarded as an essential step to realize its structure, surface functional groups, and morphology. To identify the functional groups available on CAW surface that may participate in adsorption, Fourier

Transform Infrared Spectroscopy (FT-IR) was used. Pellets of the CAW were prepared by mixing it with potassium bromide (KBr) powder. The FT-IR analyses were run in the range of 4000 to 400 cm^{-1} (Bruker Optics (TENSOR 27 series, Woodlands, TX, USA). To study the surface morphology of the CAW adsorbent, Scanning Electron Microscopy (SEM) (Hitachi, Tokyo, Japan, S-3000H) was used. Samples were coated with a thin layer of gold (JFC-1200, Akishima, Tokyo, Japan.) for enhanced conductivity prior to analysis. Brunauer-Emmett-Teller (BET) analysis was conducted to measure surface area and pore volume using a Quantachrome NOVA 4000e analyzer (Florida, USA).

Preparation of Lead (Pb) and Phenol Solutions

All chemicals utilized were purchased from Sigma-Aldrich, India and were of analytical grade. Lead nitrate ($Pb(NO_3)_2$) and phenol (C_6H_6OH) were used for the adsorbate preparations. An appropriate weight of the adsorbate (1.598 g of $Pb(NO_3)_2$ and 1 g of phenol) were dissolved in deionized water for preparation of the stock solution. Different concentrations of the pollutant solution were prepared *via* dilution of the stock solution using deionized water. Solution pH was adjusted in the range of pH 4 to 6 for optimal adsorption using 0.1M of HCL or NaOH.

Adsorption Study

Batch adsorption experiments were done through the introduction of a specific amount of calcined animal waste (ranging from 0.1 to 0.8 g) into 20 mL of contaminant solution within a conical flask. A magnetic stirrer was used to stir the mixture at a constant speed for a fixed duration of 120 min to achieve adsorption equilibrium. Afterward, separation of the adsorbent from the solution was done through filtration. The residual concentrations of lead and phenol in the supernatant were determined, respectively, using Atomic Absorption Spectroscopy (AAS) (Thermo Fisher Scientific, Waltham, MA, USA) and a UV-Visible spectrophotometer at a wavelength of 270 nm (Shimadzu, Japan). Each experiment was performed in triplicate. The adsorbent's adsorption capacity (Q_e) (mg/g) was computed using the following equation,

$$\text{Adsorption capacity, } Q_e = \frac{C_o - C_e}{m} V \quad (1)$$

$$\text{Percentage adsorbed, } Q_e(\%) = \frac{C_o - C_e}{C_o} x100 \quad (2)$$

where C_0 and C_e are the initial and equilibrium concentration of lead or phenol (mg/L), V stands for solution volume used (L), and m denotes the adsorbent mass (g). The same procedure was repeated to investigate the impact of various factors at different pH, various time intervals, temperature, initial pollutant concentration, and dosage of CAW adsorbent used.

Statistical analyses were performed using Origin software (OriginLab Corporation, Origin 2020 (9.7), Northampton, MA, USA).

Desorption Studies

To assess the feasibility of the sorption process, sorption-desorption experiments were conducted on the used adsorbent. Once equilibrium was reached, the exhausted adsorbent was carefully separated, and desorption was carried out using acetic acid. The concentration of the washed effluent was then measured using Atomic Absorption

Spectroscopy (AAS) (Thermo Fisher Scientific, Waltham, MA, USA) and a UV-Visible spectrophotometer at a wavelength of 270 nm (Shimadzu, Japan). This desorption procedure was repeated for six cycles, following the same experimental conditions, and the percentage desorption (PD) was calculated using the expression below,

$$PD(\%) = \frac{AD}{AA} X100 \quad (3)$$

where AD represents the amount of effluent desorbed (mg) and AA denotes the amount of effluent adsorbed (mg). All experiments were conducted in triplicate, and the mean values were recorded.

RESULTS AND DISCUSSIONS

FT-IR and SEM Analysis of Calcined Animal Waste

The animal waste FT-IR analysis before adsorption (Fig. 1a) revealed prominent broad peaks observed around 3325 to 3560 cm^{-1}, suggesting that hydroxyl groups were present that could originate from adsorbed water molecules or characteristic peaks of cellulose, hemicellulose, and lignin (Puri *et al*. 2020; Yang *et al*. 2023). Peaks around 1475 and 895 cm^{-1} suggest the presence of carbonate (CO_3^{2-}) groups. The C=O peak is seen at 1726 cm^{-1}, which is attributed to unconjugated ketones and is characteristic of hemicellulose vibration (Yang *et al*. 2020), while the peaks seen at 1015 cm^{-1} correspond to Si–O or C-O groups. After adsorption of lead ions (Fig. 1b), the peaks corresponding to –OH group that were seen at 3320 to 3560 cm^{-1} shifted slightly to lower wavenumbers (3250 to 3495 cm^{-1}). This shift indicates the involvement of –OH groups in hydrogen bonding or complexation with adsorbed metal ions (*e.g.*, Pb^{2+}). The C=O peak seen at 1726 cm^{-1} in the calcined material had increased to 1732 cm^{-1}, whereas the peaks around 1475 and 895 cm^{-1} shifted slightly to 1471 cm^{-1} and 892 cm^{-1}, signifying the interaction of carbonate groups with metal ions during the adsorption process. Similarly, the peaks initially seen at 1015 cm^{-1} that correspond to Si–O or C-O groups shifted to lower frequencies at 1008 cm^{-1}. The interaction between pollutants and the calcined cow dung adsorbent involved hydroxyl, carbonate, and possibly silicate groups. These groups are essential for forming bonds or coordinating with the adsorbed ions. The SEM images of calcined animal waste before adsorption (Fig. 2a) reveal a distinct presence of rod-like fibers embedded within the structure and these fibers likely represent organic components retained during the calcination process. After the adsorption process (Fig. 2b), the rod-like fibers observed before adsorption were coated with a thin layer. This coating smoothens the surface, thereby reducing the visibility of the original fibrous texture.

The BET characterization of calcined animal waste revealed its strong potential as an adsorbent for wastewater treatment, particularly for removing lead ions (Pb^{2+}) and phenol. With a high surface area of 304 m^2/g, CAW provides a large number of active sites for adsorption, enhancing its ability to capture and retain contaminants. Its pore volume of 0.158 cm^3/g indicates sufficient internal porosity, allowing effective trapping of pollutants within the adsorbent structure. Additionally, the pore diameter of 2.22 nm classifies CAW as a mesoporous material, making it well-suited for adsorbing both organic and inorganic pollutants due to its balanced pore size, which facilitates the diffusion of molecules into the adsorbent. Overall, the combination of high surface area,

adequate pore volume, and mesoporous structure suggests that CAW is a highly effective adsorbent.

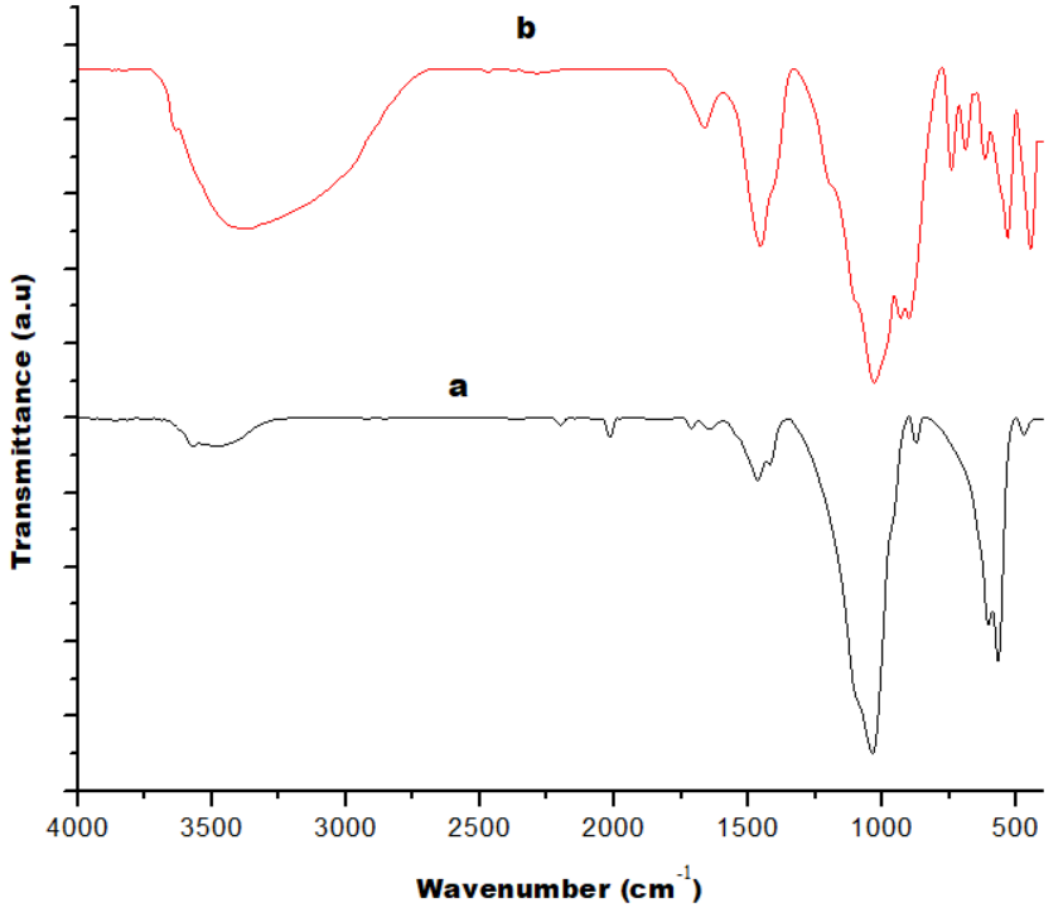

Fig. 1. FT-IR analysis of calcined animal waste (a) before and (b) after adsorption

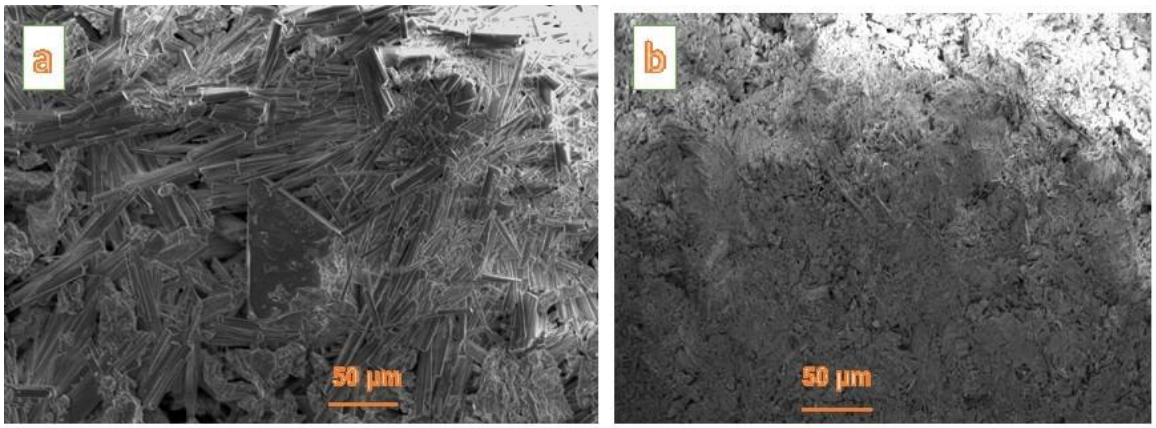

Fig. 2. SEM analysis of calcined animal waste (a) before and (b) after adsorption

Effects of Initial Metal Concentration and Contact Time

The adsorption of phenol and lead (Pb) from aqueous solutions onto calcined animal waste (CAW) is influenced by factors such as initial pollutant concentration and contact time. This study evaluated the adsorption capacity of CAW for phenol and lead

across a concentration range of 40 to 280 mg/L and contact times from 10 to 160 min (Figs. 3 and 4). At an initial concentration of 40 mg/L, phenol adsorption reached 5.30 mg/g, while lead adsorption was 7.03 mg/g after 10 min. Over time, these values increased to 9.24 mg/g for phenol and 21.0 mg/g for lead at 120 min. The initial rapid adsorption can be attributed to an abundance of vacant active sites on the CAW surface. As the process continued, the adsorption rate decreased as these sites became occupied, leading to equilibrium. Despite the slower rate, the total adsorption continues to increase over time (Mustapha *et al*. 2019; Upendra *et al.* 2023).

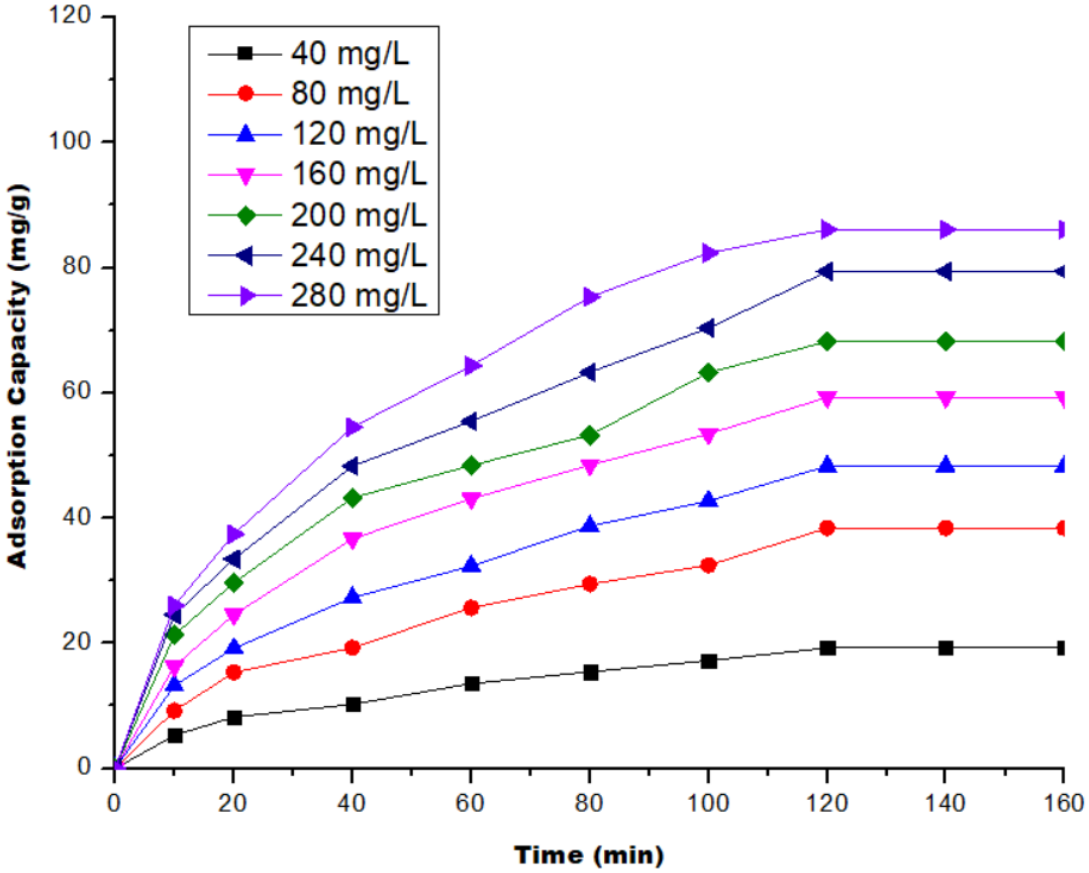

Fig. 3. Effect of contact time and pollutants concentration on the adsorption of phenol by CAW

At a higher initial concentration of 280 mg/L, the adsorption capacities were substantially greater at all contact times. For instance, phenol and lead adsorption reached 26.0 and 31.2 mg/g, respectively, at 10 min, and further increased to 86.1 and 95.7 mg/g at 120 min. This enhanced performance is attributed to the higher concentration gradient between the solution and the adsorbent surface, which intensified the driving force for adsorption. Consequently, CAW demonstrated superior pollutant removal efficiency at higher concentrations compared to lower ones (Mustapha *et al*. 2019; Upendra *et al*. 2023). The rise in the quantity of phenol and lead adsorbed with time suggests that the pollutant molecules were gradually diffusing into the porous structure of the animal waste, and more adsorption sites became occupied over time. However, the rate of increase in adsorption diminished after a certain period, indicating that the system was nearing its saturation point (Upendra *et al*. 2023). The data show that at both

concentrations, the amount of the pollutants adsorbed increased with time, but the increase was more pronounced at the higher initial concentration of 280 mg/L. This can be explained by the fact that at higher concentrations, the driving force for the adsorption process is greater, allowing more phenol and lead molecules to interact with the available adsorption sites on the calcined animal waste (Ofudje *et al*. 2020; Upendra *et al*. 2023). In contrast, at lower concentrations (40 mg/L), the adsorption sites become saturated more slowly, and as a result, the increase in adsorption with time is less substantial.

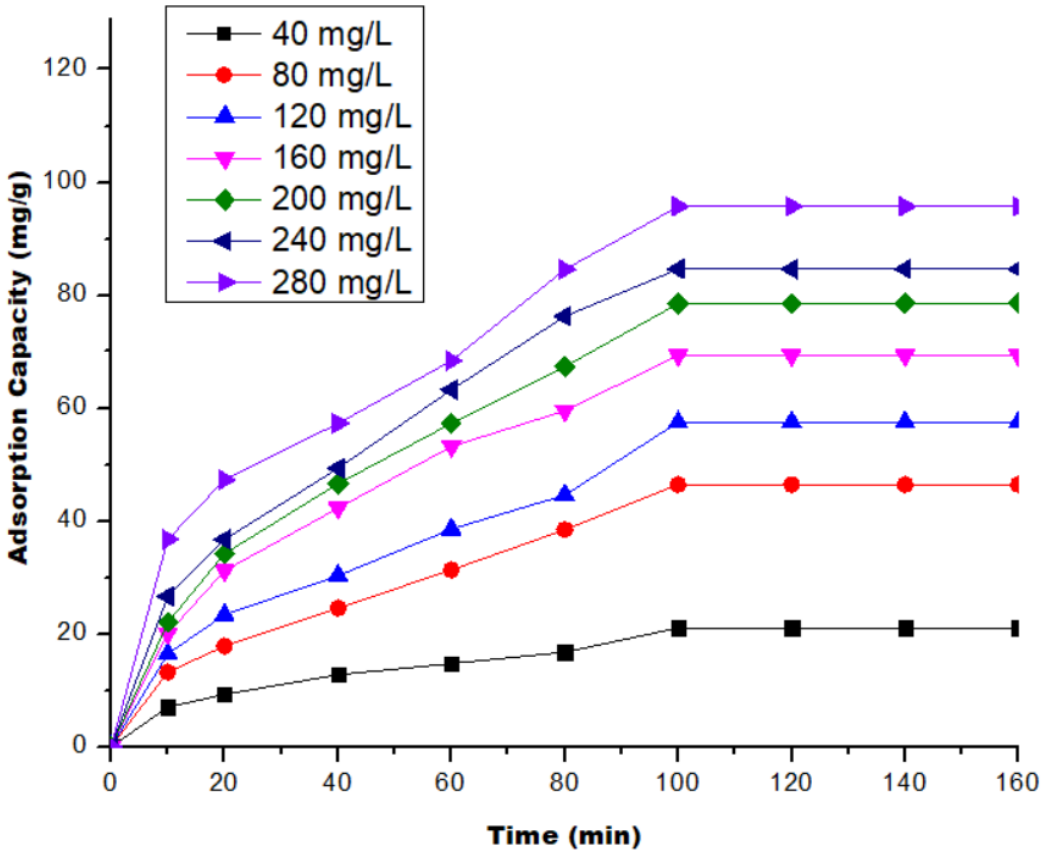

Fig. 4. Effect of contact time and pollutants concentration on the adsorption of Pb by CAW

Adsorption of Phenol and lead as a Function of pH

Solution pH is known to play a vital role in adsorption processes, influencing both the ionization state of the adsorbate and the charge on the adsorbent surface. This comparative analysis examined the effect of pH on the adsorption of phenol and lead (Pb) by calcined animal waste based on the provided data in Fig. 5. For phenol, the percentage adsorption increased from 53.7% to 75.9% as the pH rose from 1.5 to 6.5. However, at a pH of 8.5, the adsorption percentage decreased to 48.8%. However, for lead, the percentage adsorption increased from 57.9% to 82.8% as the pH rose from 1.5 to 4.5. However, at a pH of 8.5, the adsorption percentage decreased to 55.2%. The reason for the decrease in lead (Pb^{2+}) adsorption by cow dung at pH 8.5 to 55.16% could be due to the fact that at higher pH levels (above ~7 to 8), lead ions (Pb^{2+}) tend to form insoluble lead hydroxide $Pb(OH)_2$, thus reducing the availability of free Pb^{2+} ions for adsorption onto cow dung. This precipitation process competes with adsorption, leading to a decline in adsorption efficiency. Also, at higher pH, the sites for adsorption may become negatively charged, which can lead to electrostatic repulsion between $Pb(OH)_3^-$ or

$Pb(OH)_4^{2-}$ species and the adsorbent surface, thus decreasing adsorption efficiency. The value of the point of zero charge (pHpzc) for the calcined animal waste adsorbent was determined to be 4.3 and above this value, the surface charge of the adsorbent shifts from positive to negative, affecting the adsorption behavior of both phenol and lead. In the case of lead adsorption for instance, the increase in adsorption from 57.9% to 82.8% as pH rose from 1.5 to 4.5 suggests that at lower pH levels, the adsorbent surface was positively charged, leading to electrostatic repulsion between Pb^{2+} ions and the surface. However, as pH approached 4.5, the surface charge became higher than the pHpzc, allowing for increased Pb^{2+} binding due to reduced repulsion and stronger complexation with available functional groups. Beyond pH 4.5, lead adsorption may decrease (as observed at pH 8.5 with only 55.2% adsorption) due to the formation of insoluble $Pb(OH)_2$ precipitates, reducing the number of free Pb^{2+} ions available for adsorption.

For phenol adsorption, the increase in phenol adsorption from 53.7% to 75.9% as pH rose from 1.5 to 6.5 indicates that phenol adsorption benefited from a more negatively charged adsorbent surface. Since phenol is a weak acid (pKa ~9.9), at lower pH, it remains largely non-ionized, making adsorption more dependent on hydrophobic interactions rather than electrostatic attraction. At pH 6.5, the surface is largely negatively charged (above pHpzc), leading to enhanced adsorption due to hydrogen bonding or π-π interactions. However, at pH 8.5, adsorption decreased (48.8%). This is attributed to the fact that phenol molecules may deprotonate, becoming negatively charged (phenolate ion), leading to electrostatic repulsion from the negatively charged adsorbent surface (Mishra *et al*. 2019; Haitham *et al*. 2022).

Mishra *et al.* (2019) in a study on phenol adsorption by activated carbon of corn husk origin, noted that the percentage removal of the activated carbon prepared at 250 °C, phenol increased from 55% to 81% as the pH increased from 4 to 6, whereas, for the adsorbent derived at 500 °C, the removal efficiency increased from 78% to 98% when the pH was increased from 4 to 7.l

Haitham *et al*. (2022) investigated phenol adsorption using a lignocellulose-derived activated carbon from agricultural wastes and noted a rise in adsorption capacity as the pH was increased from 2 to 4. This enhancement could have been related to electrostatic interactions, where the positive surface charge of the activated carbon attracted the adsorbate molecules at pH 2. However, at pH levels above 4, the adsorption efficiency declined due to electrostatic repulsion between the negatively charged carbon surface.

In the case of the lead ions, at lower pH levels, the adsorbent surface was likely protonated, which limited lead adsorption due to electrostatic repulsion between positively charged lead ions and the protonated surface of CAW. As the pH was increased to 4.5, this competition diminished, and the lead ions were able to bind more effectively to the negatively charged functional groups on the CAW. Both adsorbates experienced reduced adsorption at pH 8.5. For phenol, this is due to ionization and repulsion, whereas for lead, it is due to hydroxide precipitation (*e.g.*, $Pb(OH)_2$) and increased repulsion.

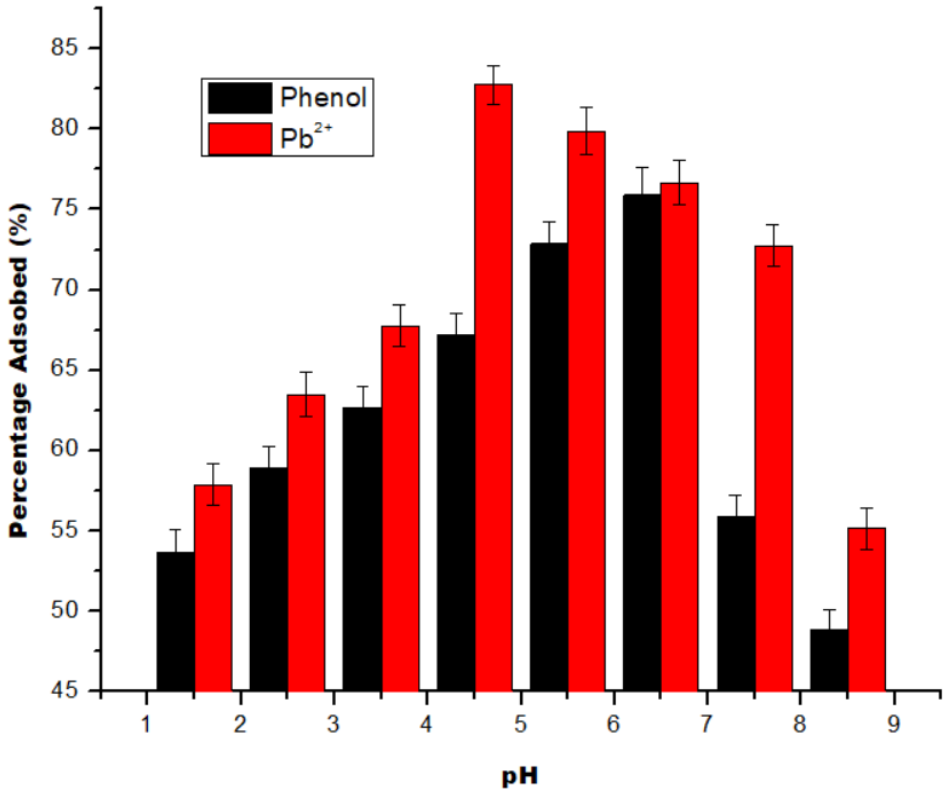

Fig. 5. Function of pH on the removal of phenol and lead ions by CAW

Effects of Adsorbent Dosage

The adsorbent dosage plays a crucial role in the adsorption process, as it determines the availability of active sites for the adsorbate and influences the overall efficiency of pollutant removal. In this study, the effect of calcined biomass dosage on the adsorption of phenol and lead (Pb) was evaluated, as illustrated in Fig. 6. For phenol, the adsorption percentage increased from 52.5% to 78.0% as the dosage of calcined animal waste (CAW) biomass increased from 0.1 g to 0.6 g, before declining to 68.8% at a dosage of 0.8 g. Similarly, for lead, the adsorption percentage rose from 56.1% to 84.2% as the biomass dosage increased from 0.1 g to 0.5 g, and then it decreased to 75.8% at 0.8 g. The initial rise in adsorption efficiency with increasing dosage can be attributed to the greater availability of active sites on the surface of the calcined biomass, providing more opportunities for the pollutants to bind (Mustapha *et al*. 2019; Akinhanmi *et al*. 2020; Ademoyegun e*t al*. 2022).

Additionally, at higher dosages, there is less competition between adsorbate molecules for the adsorption sites, which facilitates greater removal. At higher dosages (0.8 g), the adsorption percentage began to decrease slightly. This could be due to saturation of adsorption sites, as a large portion of its adsorption sites is already occupied, and the additional biomass does not provide a corresponding increase in available sites (Mustapha *et al*. 2019; Ofudje *et al*. 2020). Both phenol and lead exhibited increased adsorption with increasing biomass dosage, but the optimal dosage for phenol (0.6 g) was slightly higher than for lead (0.5 g). Mishra *et al.* (2019) observed similar behavior during phenol adsorption studies using activated carbon derived from corn husk. They observed that increasing the dosage to 3 g/L had little to no impact on the removal

efficiency and, in some cases, caused a slight decrease. They attributed this to the agglomeration of adsorbent particles at higher concentrations, which resulted in larger particle sizes and a subsequent reduction in the specific surface area and available active binding sites.

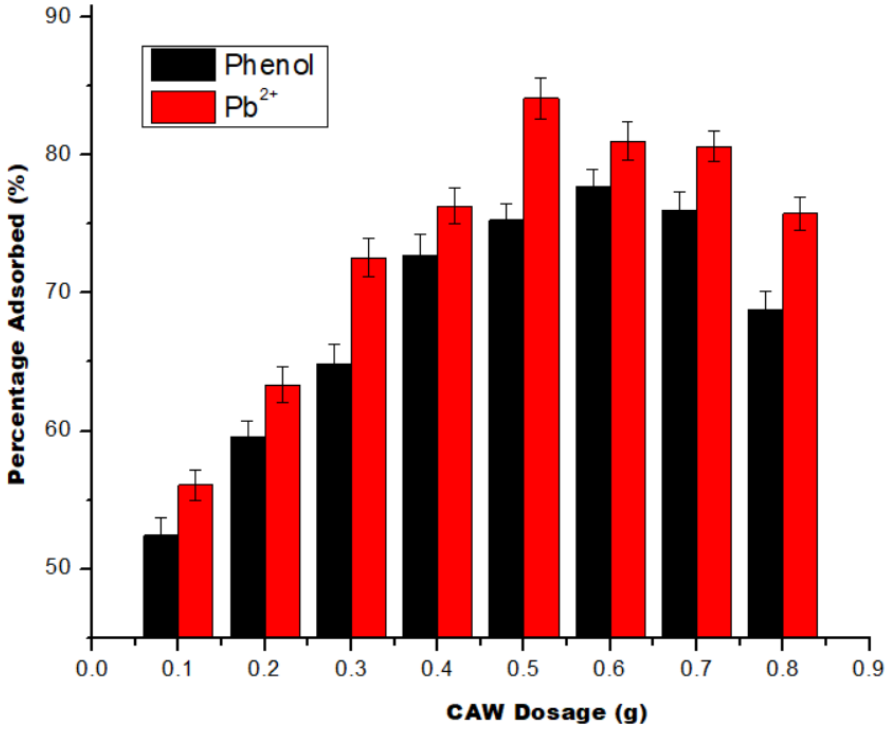

Fig. 6. Function of CAW dosage on the removal of phenol and lead ions by CAW

Effects of Temperature

Temperature plays a crucial role in determining the rate and extent of adsorption. The effect of temperature on the adsorption process depends on the characteristics of both the adsorbent and the adsorbate. The analysis of how temperature affects the adsorption of phenol and lead (Pb) by calcined animal waste is shown in the data provided in Fig. 7. For phenol, the percentage of adsorption increased from 54.2% at 25 °C to 79.8% at 45 °C, and then it decreased to 75.9% at 60 °C. For lead (Pb), the percentage of adsorption increased from 59.8% at 25 °C to 87.2% at 50 °C, and then it remained constant thereafter. The rise in adsorption with temperature from 25 °C to 45 °C or 50 °C is likely due to the increased kinetic energy of the pollutant molecules. Additionally, at higher temperatures, the number of available adsorption sites on the calcined animal waste might increase, or the surface energy of the adsorbent could improve, leading to more efficient phenol and lead ions adsorption. At higher temperatures (60 °C), the physical structure of adsorbent might start to degrade, reducing the number of active sites available for adsorption and heat may cause some of the adsorbed contaminant molecules to desorb from the adsorbent surface (Sobik-Szołtysek *et al*. 2021). This phenomenon might have explained why adsorption processes at elevated temperatures leads to decrease in the uptake process.

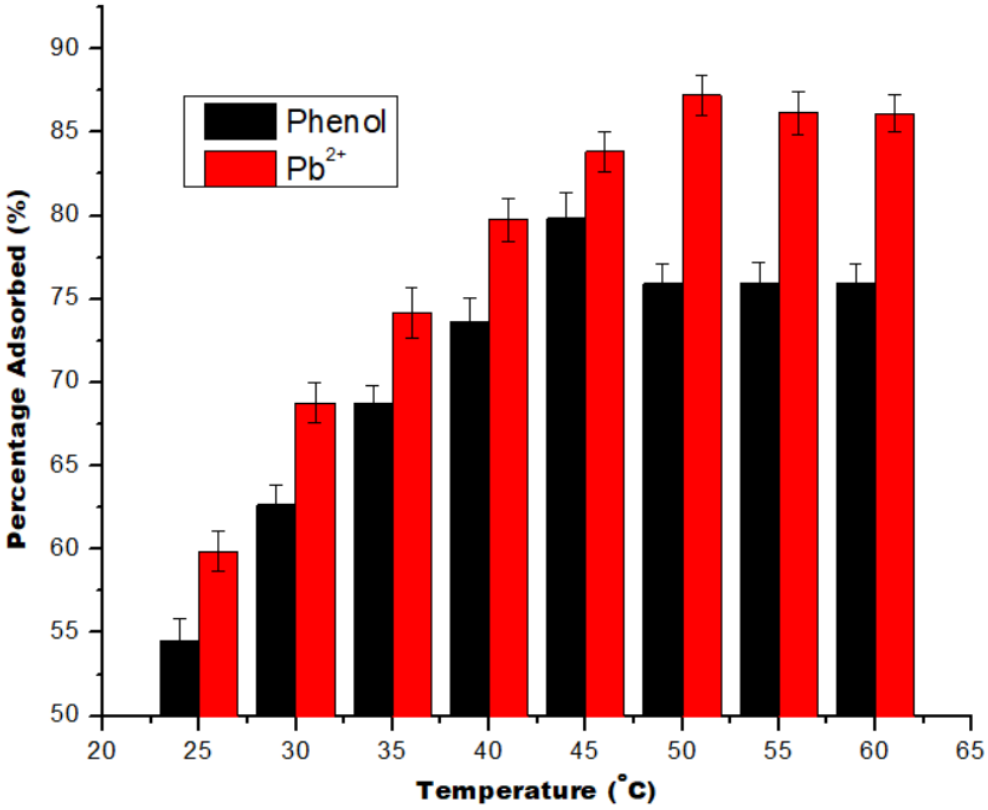

Fig. 7. Function of temperature on the removal of phenol and lead ions by CAW

Comparatively, both phenol and lead showed an increase in adsorption with rising temperature, but phenol showed a slight decrease at 60 °C, while lead adsorption reached a maximum at 50 °C and did not change with further increases in temperature. The optimal temperature for phenol adsorption was 45 °C, whereas for lead it was 50 °C and this difference suggests that the adsorption processes for phenol and lead are not identical and may involve different mechanisms or binding energies.

Kinetics Examinations

Pseudo-first-order kinetic model

The pseudo-first-order kinetic model (PFOKM) presumes that the rate of adsorption is directly proportional to the number of unoccupied sites. The linear equation form of the model and the key parameters analyzed include (Mustapha *et al*. 2019; Haitham *et al*. 2022),

$$In(q_e - q_t) = Inq_t - k_1 t \quad (4)$$

where $q_{e\ exp}$ and $q_{e\ cal}$ are the experimentally and calculated determined equilibrium adsorption capacity (mg/g), respectively, and k_1 is the rate constant for PFOKM (min^{-1}). The Sum of Squared Errors (% SSE) measures the difference between experimental and calculated values and lower values indicate better accuracy. The expression for this error analysis is given in the equation below (Ofudje *et al*. 2017; Ogundiran *et al*. 2022):

$$\%SSE = \sqrt{\frac{(q_{(\exp)} - q_{(cal)})^2}{N}} \quad (5)$$

The values obtained from the plots in Fig. 8a are shown in Table 1. Both adsorbates showed strong adherence to the PFOKM based on the values of R^2, but phenol adsorption exhibited a slightly better and more consistent fit. This view is supported from the values of % SSE, with phenol adsorption showing lower % SSE values, suggesting that the PFOKM better predicted its adsorption behavior compared to lead. This was also corroborated by the closeness in the values of the experimental adsorption capacity when compared with the calculated adsorption capacity for phenol. Lead exhibited higher k_1 values, implying a faster approach to equilibrium, possibly due to the ionic nature of lead ions, which facilitates quicker binding to active sites.

Table 1. Parameters of Kinetic for Phenol and Lead Adsorption by CAW

		Phenol						
Pseudo-first order	C_o (mg/L)	40	80	120	160	200	240	280
	$Q_{e\ exp}$ (mg g^{-1})	19.2	38.4	48.30	59.3	68.2	79.4	87.465
	$Q_{e\ cal}$ (mg g^{-1})	19.1	38.0	45.0	61.1	69.2	83.0	88.0
	k_1 (min^{-1})	0.015	0.024	0.076	0.113	0.224	0.598	1.025
	R^2	0.998	0.997	0.994	0.989	0.996	0.997	0.998
	% SSE	0.004	0.005	0.030	0.014	0.007	0.020	0.003
Pseudo-second order	$Q_{e\ cal}$ (mg g^{-1})	32.8	45.3	56.3	76.3	82.7	85.3	97.0
	k_2 (g mg^{-1} min^{-1})	0.479	0.562	0.741	1.061	1.384	2.372	3.026
	R^2	0.955	0.946	0.963	0.977	0.970	0.958	0.976
	% SSE	0.316	0.081	0.074	0.128	0.095	0.033	0.049
Intra-particle diffusion	K_p (mg g^{-1} min$^{-0.5}$)	1.648	1.937	3.264	7.074	9.345	13.089	15.204
	C_1 (mg g^{-1})	0.075	1.894	3.159	4.586	5.042	5.893	6.362
	R^2	0.987	0.994	0.984	0.994	0.955	0.963	0.978
		Pb						
Pseudo-first order	C_o (mg/L)	40	80	120	160	200	240	280
	$Q_{e\ exp}$ (mg g^{-1})	21.0	46.4	57.5	69.3	78.5	84.6	95.7
	$Q_{e\ cal}$ (mg g^{-1})	27.2	41.9	49.7	80.3	94.1	101.5	113
	k_1 (min^{-1})	0.155	0.475	0.732	1.279	1.324	1.613	2.105
	R^2	0.998	0.986	0.994	0.968	0.956	0.981	0.936
	% SSE	0.132	0.043	0.061	0.071	0.089	0.089	0.081
Pseudo-second order	$Q_{e\ cal}$ (mg g^{-1})	20.7	46.0	54.1	71.0	79.0	82.1	97.0
	k_2 (g mg^{-1} min^{-1})	0.202	0.443	0.725	1.451	1.524	1.714	2.241
	R^2	0.989	0.996	0.993	0.997	0.987	0.989	0.996
	% SSE	0.008	0.004	0.027	0.011	0.003	0.013	0.006
Intra-particle diffusion	K_p (mg g^{-1} min$^{-0.5}$)	8.02	10.9	18.1	25.0	31.7	33.2	39.0
	C_1 (mg g^{-1})	0.328	0.624	0.947	1.228	1.831	2.093	2.836
	R^2	0.987	0.988	0.989	0.944	0.995	0.963	0.974

Pseudo-Second-Order Kinetic Model

The pseudo-second-order kinetic model can be represented by the expression in Eq. 5 (Mustapha *et al*. 2019; Haitham *et al*. 2022):

$$t/q_t = 1/k_2 q_e^2 + 1/q_e t \quad (6)$$

where k_2 is the rate constant for the pseudo-second-order adsorption (g/mg·min), and all other parameters are as previously defined. The plot for this model is shown in Fig. 8b, and its values are presented in Table 1. Both adsorbates showed substantial adsorption capacities, but lead had more consistent experimental and calculated q_e values, whereas phenol showed a larger variation between the experimental and calculated values, indicating potential complexities in its adsorption process. Regarding the strength of R^2, lead adsorption generally showed a better fit to the PSOKM, with higher values, suggesting that the adsorption process for lead is more homogeneous and follows a second-order kinetic model more closely than phenol. Additionally, lead adsorption showed a lower % SSE, which means the PSOKM is a more accurate predictor for lead adsorption compared to phenol, though the model can still be applicable to phenol.

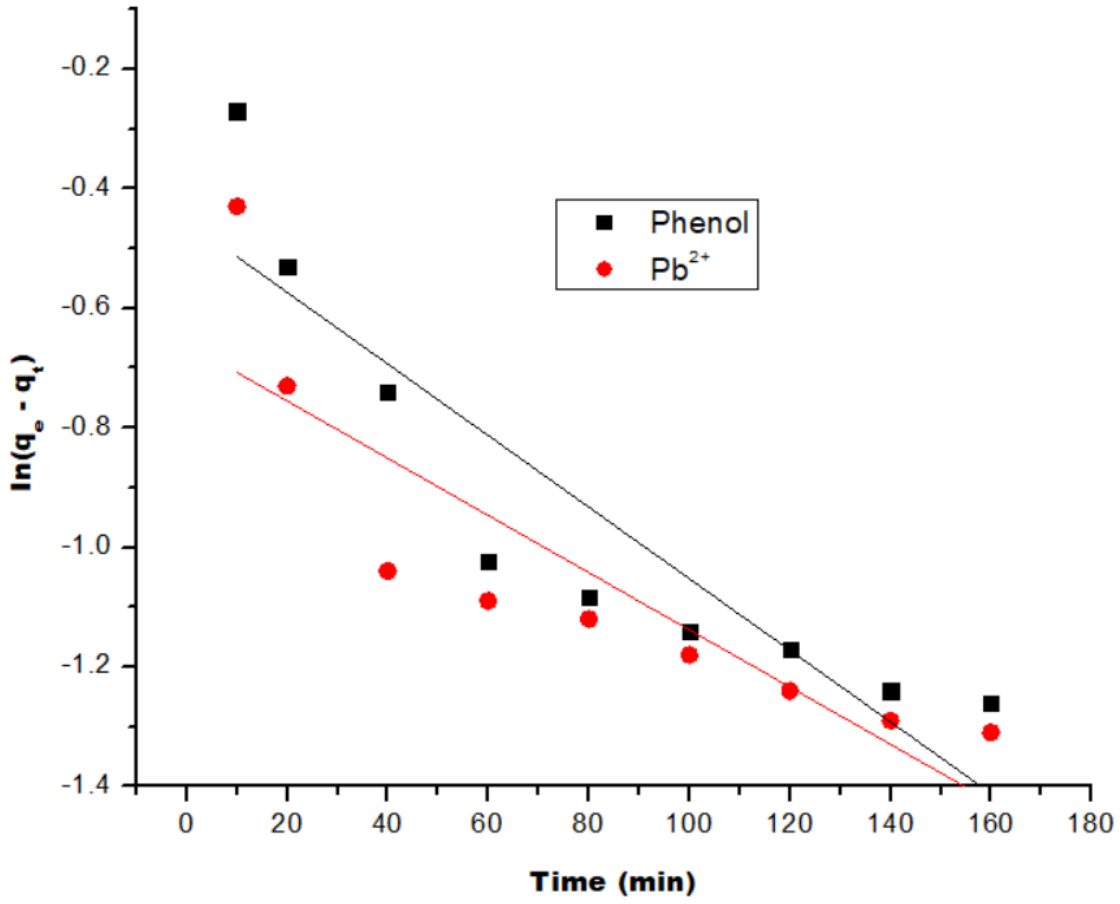

Fig. 8a. Kinetic plots of pseudo-first-order for phenol and lead adsorption by CAW

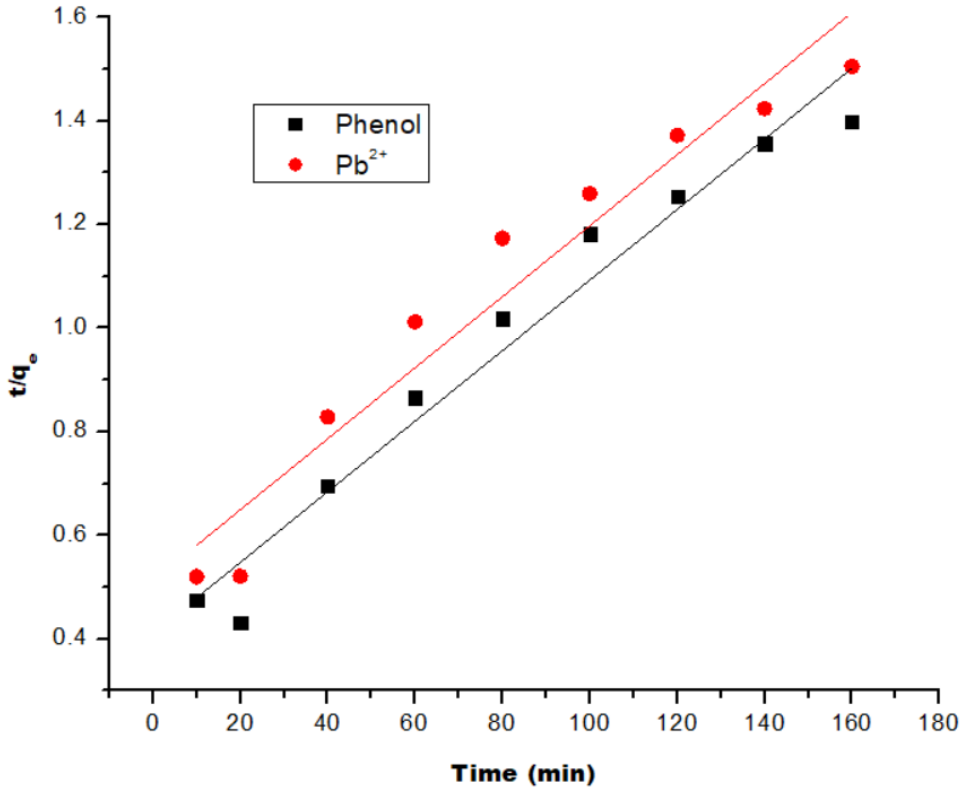

Fig. 8b. Kinetic plots of pseudo-second-order for phenol and lead adsorption by CAW

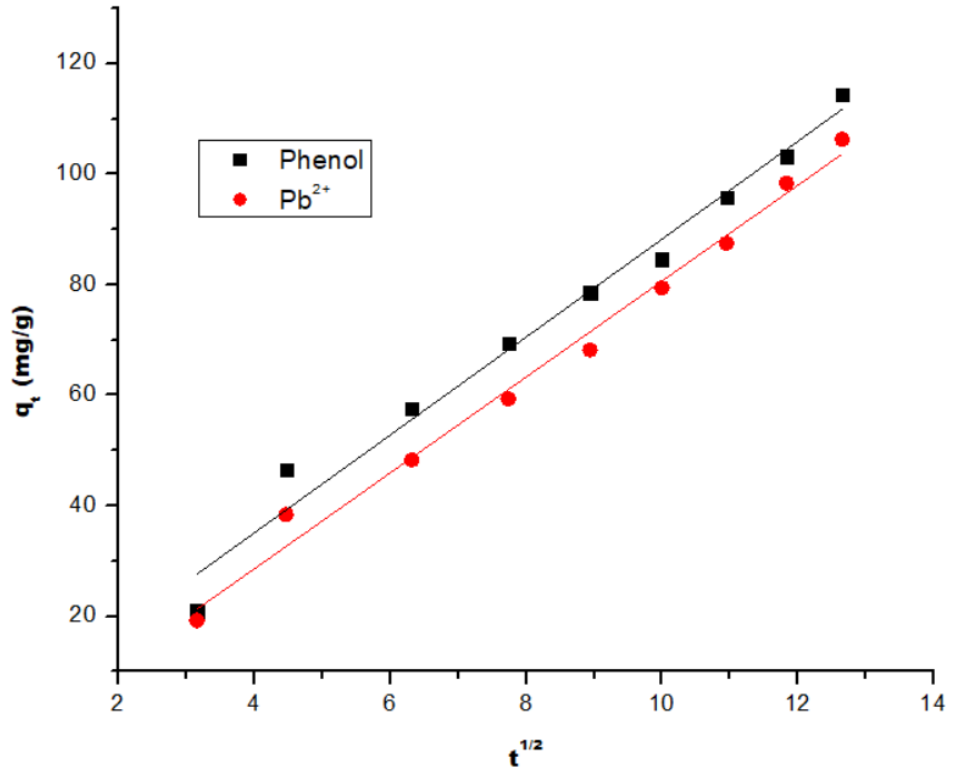

Fig. 8c. Kinetic plots of intra-particle diffusion for phenol and lead adsorption by CAW

Intra-Particle Diffusion Kinetics Model

The intra-particle diffusion model is often used to describe the rate-limiting step of adsorption, which is the diffusion of adsorbate molecules into the pores of the adsorbent. The key parameters and the linear form of this model are calculated using Eq. 6 (Ofudje *et al*. 2017; Ogundiran *et al*. 2022).

$$Q_t = K_p t^{1/2} + C_i \quad (7)$$

In Eq. 7, K_p denotes the Intra-particle diffusion rate constant (mg/g·min$^{1/2}$), which represents the rate at which the adsorbate diffuses into the biochar particles, and C_i is the intercept, which is indicative of the initial concentration gradient and can suggest whether the adsorption is controlled by diffusion within the particles or surface adsorption. The parameters were deduced from the plots represented in Fig. 8c, and their values are listed in Table 1. For lead adsorption, the values of the K_p ranged from 8.02 to 39.0 mg/g·min$^{1/2}$, indicating a relatively higher rate of diffusion into the pores of the biochar, suggesting that lead ions are diffusing more efficiently through the biochar structure. In the case of phenol adsorption, the values of the K_p ranged from 1.65 to 15.2 mg/g·min$^{1/2}$, which is lower than for lead, indicating that phenol diffusion into the biochar particles was slower compared to lead ions. Phenol showed a higher C_i than for lead ions indicating a higher concentration gradient, particularly at lower concentrations and this suggests that for phenol, the adsorption process might involve a stronger surface interaction before diffusion occurs. Both phenol and lead showed good fits to the intra-particle diffusion model with high R^2 values, coupled with strong correlation with the PFOKM, and with the PSOKM. This indicates that the adsorption rate is primarily controlled by the diffusion and interaction of adsorbate molecules occurs within a porous network (Hubbe *et al*. 2019). This suggests that pore diffusion and surface interactions within the adsorbent structure play a significant role in governing the adsorption process.

Adsorption Isotherms

Langmuir isotherm model

The Langmuir isotherm model is widely used to describe adsorption processes that occur on homogeneous and finite adsorption sites, where each site can hold only one adsorbate molecule or ion (Langmuir 1918; Haitham *et al*. 2022). The Langmuir equation and the key parameters of the isotherm include (Langmuir 1918; Haitham *et al*. 2022) the following:

$$\frac{C_e}{q_e} = \frac{1}{Q_m b} + \frac{1}{Q_m} C_e \quad (8)$$

The separation factor or dimensionless constant (R_L) is also given as (Mustapha *et al*. 2019),

$$R_L = \frac{1}{(1 + bC_i)} \quad (9)$$

where C_i stands for initial adsorbate concentration (mg L^{-1}). These constants were evaluated from Fig. 9a and their values are listed in Table 2. Q_{max} is the maximum adsorption capacity, representing the total amount of adsorbate required to form a complete monolayer on the adsorbent surface in mg/g, and R_L is the separation factor, which indicates the favorability of the adsorption process.

Table 2. Parameters of Isotherms for Phenol and Lead Adsorption by CAW

Isotherms	Parameters	Phenol	Lead (Pb)
Langmuir	Q_{max} (mg/g)	89.34	101.242
	R_L (mg/L)	0.221	0.071
	R^2	0.956	0.998
Freundlich	K_F (mg/g)	48.115	55.613
	1/*n*	0.335	0.177
	R^2	0.998	0.984
Temkin	K_T (L g^{-1})	0.502	0.565
	B (J mol^{-1})	26.213	33.948
	R^2	0.959	0.966
Dubinin-Radushkevich	Q_s (mg/g)	47.362	66.052
	E (kJ/mol)	4.205	10.196
	R^2	0.970	0.976

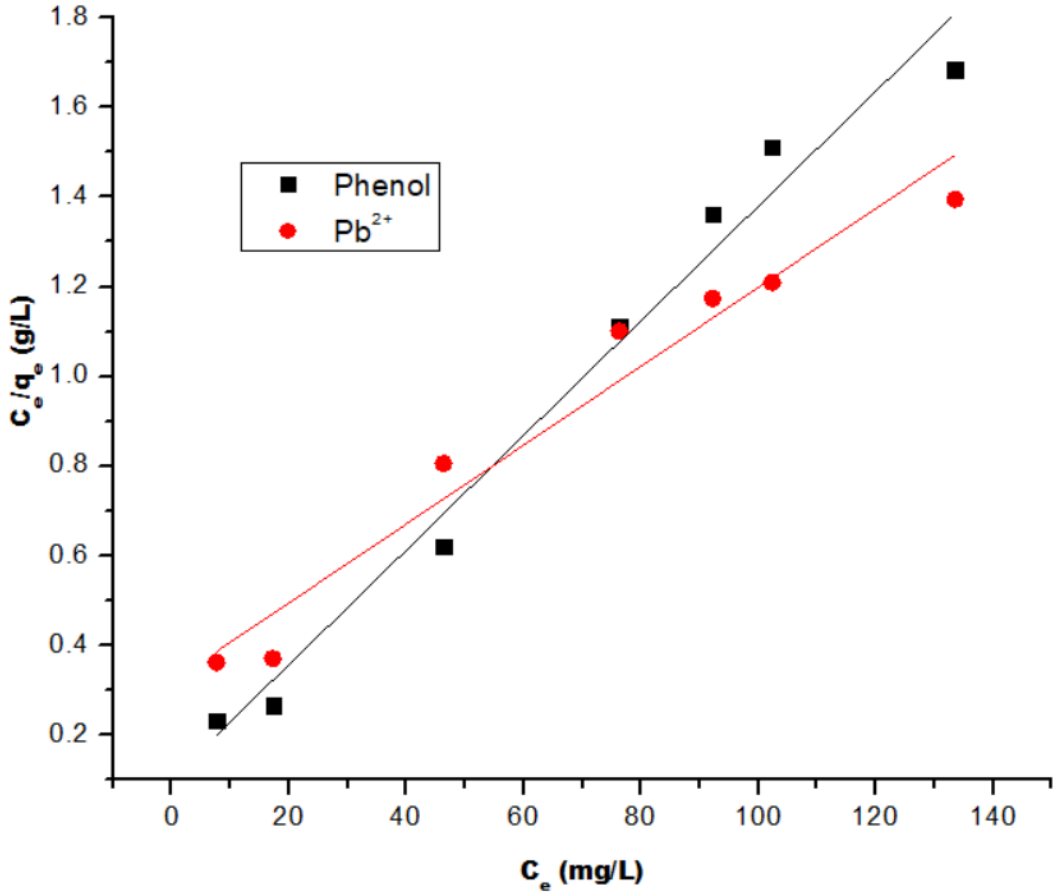

Fig. 9a. Plot of Langmuir on the adsorption of phenol and lead ions by CAW

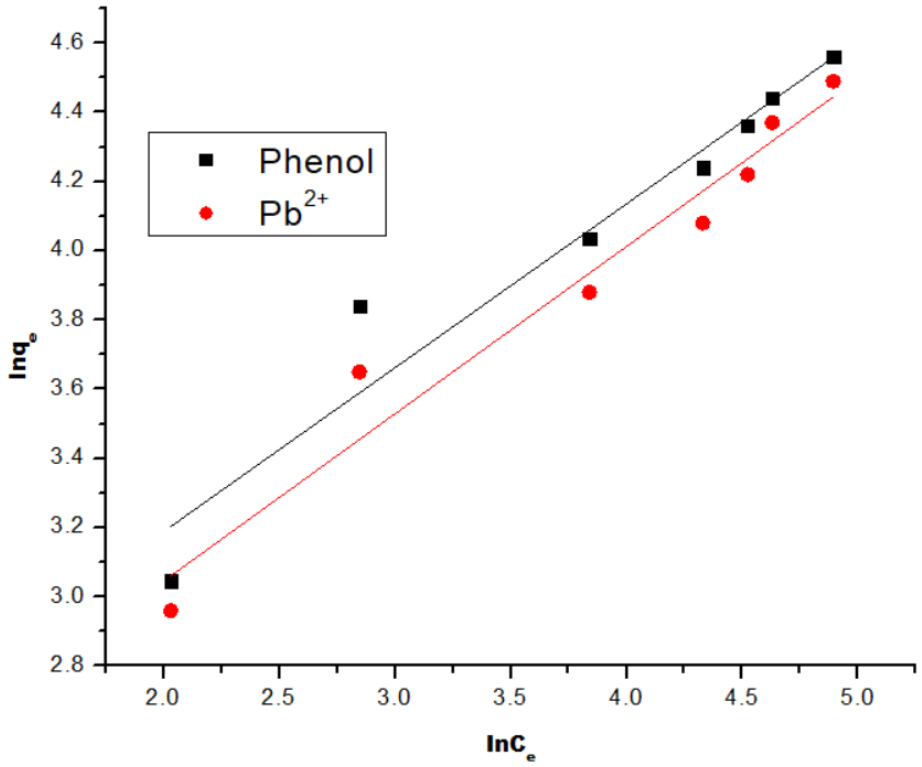

Fig. 9b. Plot of Freundlich on the adsorption of phenol and lead ions by CAW

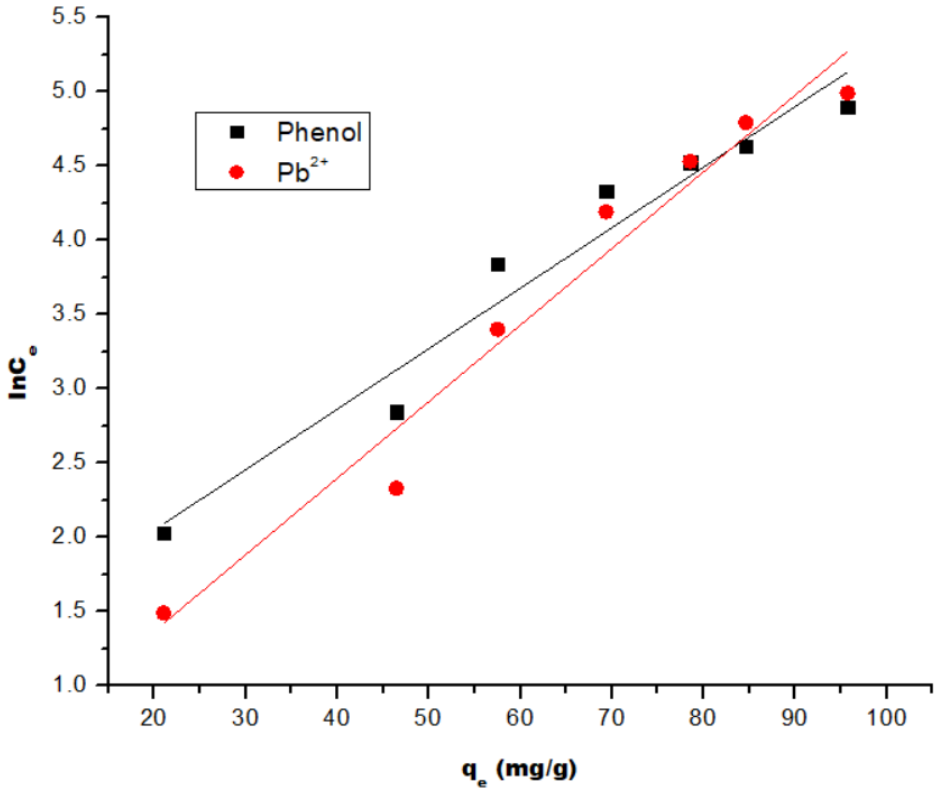

Fig. 9c. Plot of Temkin on the adsorption of phenol and lead ions by CAW

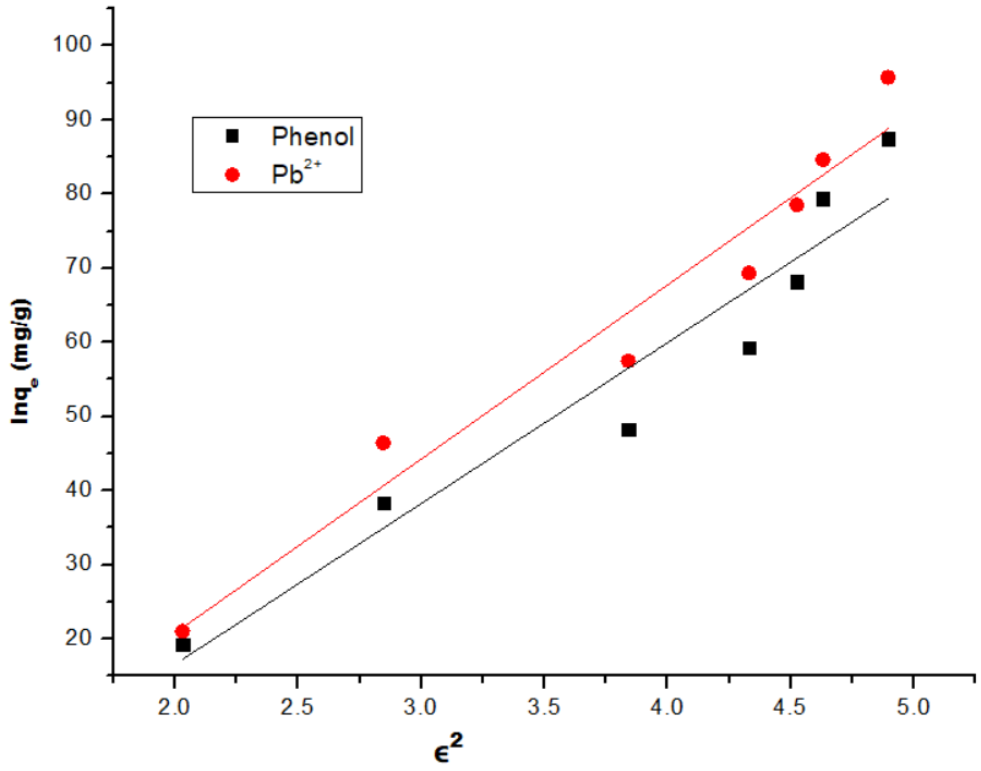

Fig. 9d. Plot of Dubinin-Radushkevich on the adsorption of phenol and lead ions by CAW

The higher Q_{max} (101 mg/g) for lead suggests that calcined animal waste had a greater capacity for lead adsorption than for phenol, for which Q_{max} was 89.3 mg/g. This may be due to the fact that the adsorbent had more affinity towards lead ions when compared with phenol. The R_L value for phenol and lead were 0.221 and 0.071, respectively, indicating highly favorable adsorption especially for the lead ions. This might be due to the compatibility of the calcined animal waste surface with phenol molecules, potentially influenced by molecular size, shape, and specific interactions. While both adsorbates showed strong adherence to the Langmuir isotherm, lead adsorption exhibited a better fit based on the values of the coefficient of determination (R^2) compared to phenol. This suggests that lead adsorption may more closely follow the assumptions of the Langmuir model, including homogeneous sites and independent interaction of adsorbate molecules with the sites.

Freundlich Isotherm Model

This model describes sorption on heterogeneous surfaces and assumes multilayer sorption in which adsorption heat and affinities over the surface distribution is not uniform. The equation and the key parameters of the Freundlich model include (Freundlich 1906; Mustapha *et al*. 2019),

$$Inq_e = InK_F + \frac{1}{n} InC_e \quad (10)$$

where K_f denotes the Freundlich constant, representing the adsorption capacity of the adsorbent, and $1/n$, which is the adsorption intensity, indicates the favorability of the

adsorption process. The parameters were deduced from Fig. 9b and their values listed in Table 2.

The K_f value for phenol was 48.1, while that of lead was 55.6, indicating that the adsorption capacity of CAW for phenol was lower than that for phenol. The higher K_f value for lead suggests that CAW had a greater overall capacity to adsorb lead ions compared to phenol and this may be due to the stronger electrostatic interactions between the negatively charged functional groups on cow dung and the positively charged lead ions. Comparing the adsorption intensity ($1/n$) shows that the calcined animal waste had a stronger adsorption affinity for lead ions compared to phenol. This difference might arise from the nature of the interaction, with lead ions forming stronger bonds with the functional groups on the calcined animal waste surface than the weaker Van der Waals or hydrophobic interactions with phenol. Both phenol and lead adsorption processes aligned well with the Freundlich isotherm model, but phenol adsorption exhibits a slightly better fit (R^2 = 0.998). This suggests that phenol adsorption on CAW might involve a more heterogeneous surface distribution of adsorption sites compared to lead adsorption.

Temkin Isotherm Model

This model assumes that the adsorption heat declines linearly with surface coverage due to these interactions (Al-Ghouti and Da'ana 2020). The equation and the key parameters of the Temkin isotherm include (Günay *et al*. 2007; Al-Ghouti and Da'ana 2020),

$$q_e = {RT}/{b_T}\, InK_T + {RT}/{b_T}\, InC_e \quad (11)$$

where K_T is the Temkin constant related to the binding energy of adsorption as higher values for this constant indicate stronger binding between the adsorbate and the adsorbent, and RT/b_T which can be represented by B is the Temkin constant related to the heat of adsorption. Here larger RT/b_T values suggest stronger adsorption interactions. These parameters presented in Table 2 were obtained from the information described in Fig. 9c.

The slightly higher K_T value for lead (0.565) suggests stronger initial interactions with lead ions compared to phenol molecules (0.502). This might be due to specific adsorption mechanisms, such as electrostatic interactions, that play a more significant role in phenol adsorption. The higher B value for lead (B = 33.9) suggests that the adsorption process for lead involves stronger overall interactions, likely due to electrostatic attractions between the negatively charged functional groups on CAW and the positively charged lead ions when compared with phenol (B = 26.2). Both adsorption processes align well with the Temkin model, but lead adsorption exhibits a slightly stronger adherence (R^2 = 0.966) than phenol adsorption (R^2 = 0.959). This suggests that the Temkin assumptions about adsorbate-adsorbate interactions are slightly more applicable to lead adsorption.

Dubinin-Radushkevich (D-R) Isotherm Model

The Dubinin-Radushkevich (D-R) isotherm model describes adsorption processes based on the porosity of the adsorbent and the energy of adsorption and it is particularly useful for distinguishing between physical and chemical adsorption mechanisms (Samarghandi *et al*. 2009). The equation and the key parameters of the D-R isotherm include (Samarghandi *et al*. 2009; Al-Ghouti and Da'ana 2020),

$$Inq_e = q_S - K\varepsilon^2 \quad (12)$$

$$\varepsilon = RTIn(1 + {}^{1}\!/_{C_e}) \quad (13)$$

$$E = {}^{1}\!/_{\sqrt{2K_{DR}}} \quad (14)$$

where Q_s is the theoretical adsorption capacity (mg/g), representing the amount of adsorbate that can be adsorbed by the adsorbent, Polanyi potential is given as ε and E denote the mean free energy of adsorption (kJ/mol). The values obtained from the plots in Fig. 9c are listed in Table 2.

The Q_s value for phenol and lead ions are 47.4 mg/g and 66.1 mg/g, respectively, with the value for lead significantly higher than that for phenol and this could be due to stronger electrostatic interactions between lead ions and the functional groups on the cow dung surface. The E value for phenol was 4.20 kJ/mol and falls within the range for physisorption, for lead ions, the value was 10.2 kJ/mol, which is indicative of chemisorption (Ofudje *et al* 2017). Regarding the strength of R^2 value, both phenol and lead adsorption processes conformed well to the D-R isotherm model, but lead adsorption exhibited a slightly better fit ($R^2 = 0.976$). This suggests that the assumptions of the D-R model, such as energy distribution across adsorption sites, align more closely with lead adsorption behavior. Table 3 revealed the effective performance of calcined cow waste adsorption capacity with others in literature towards the adsorption of lead and phenol.

Table 3. Comparative Performance of the Adsorption Capacity of Calcined Cow Waste with Previous Literature

Pb^{2+} (mg/g)		
Modified chitosan/Vermiculite adsorbents	98.5	Salih *et al*. (2022)
Pottery granules	9.47	Mohammad *et al*. (2023)
Carbon materials	26.5	Kucherova *et al.* (2017)
Lignin-grafted carbon nanotubes	23.6	Li *et al.* (2017)
Dijah-Monkin bentonite clay	8.7	Alexander *et al*. (2018)
Lignite	61.4	Mlayah *et al*. (2021)
Carbon nanoparticle impregnated on clay aggregate	22.8	Ghahremani *et al*. (2021)
Shanghai silty clay	26.5	Wang and Zhang (2021)
Calcined cow dung	101.2	This study
Phenol (mg/g)		
Modified chitosan/Vermiculite adsorbents	67.1	Salih *et al*. (2022)
Multiwalled carbon nanotubes	32.2	Abdel-Ghani *et al*. (2015)
Hexamethylene bis-pyridinium dibromides	41.9	Luo *et al*. (2015)
Garlic peel	14.5	Muthamilselvi *et al*. (2016)
Acid-treated pyrolytic tire char	51.9	Makrigianni *et al*. (2015)
Phragmites australis	29.6	Shi *et al*. (2018)
Corn husk activated carbon	7.8	Mishra *et al*. (2019)
Calcined cow dung	89.3	This study

Analysis of Thermodynamic Constants

The parameters deduced from the thermodynamic investigation, such as free energy change ($\Delta G°$), enthalpy change ($\Delta H°$), and entropy change ($\Delta S°$), offer insights into the spontaneity, energy requirements, and disorder during the adsorption process.

These parameters for phenol and lead adsorption were obtained using the equations below (Adeogun *et al*. 2012; Strachowski and Bystrzejewski 2015; Mustapha *et al*. 2019),

$$K_d = \frac{q_e}{C_e} \quad (15)$$

$$\Delta G^o = -RT \ln K_D \quad (16)$$

$$\ln K_d = \Delta S^o / R - \Delta H^o / RT \quad (17)$$

where K_d is the equilibrium constant. The parameters were deduced from Fig. 10, and their values depicted in Table 5.

The $\Delta G°$ for phenol and lead ranged from -1.04 to -7.65 kJ/mol, and from -0.92 to -5.03 kJ/mol, suggesting a spontaneous process (Strachowski and Bystrzejewski 2015; Mustapha *et al*. 2019). The values of $\Delta H°$ for phenol and lead were 11.6 and 21.7 kJ/mol, indicating that the adsorption process was endothermic, requiring heat to proceed (Strachowski and Bystrzejewski 2015; Mustapha *et al*. 2019). The higher $\Delta H°$ for lead suggests that its adsorption requires more energy input, which could be due to stronger interactions or additional energy needed to overcome specific binding mechanisms. The values of $\Delta S°$ obtained were 3.56 and 5.83 J/mol·K phenol and lead, reflecting a little rise in randomness at the solid-liquid interface during adsorption.

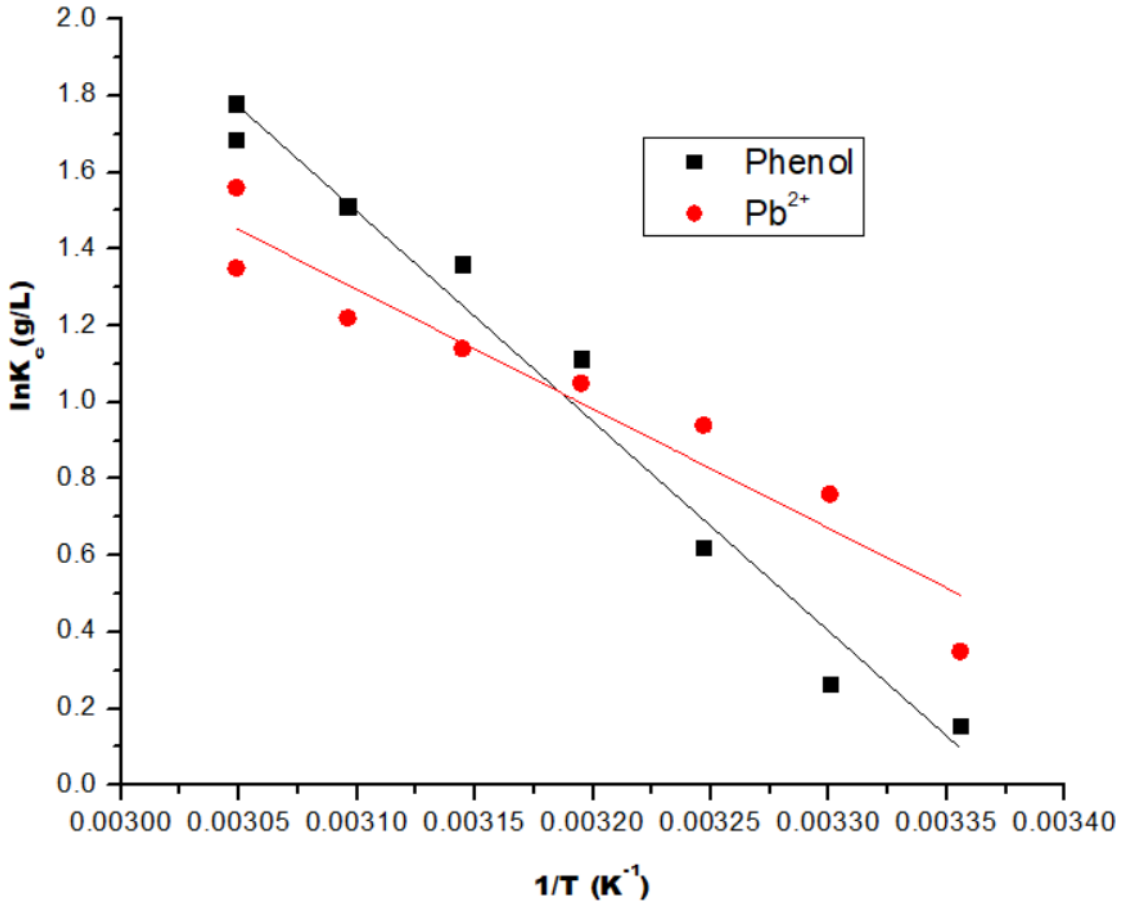

Fig. 10. Thermodynamic plots for phenol and lead adsorption by CAW

Table 5. Analysis of the Parameters from Thermodynamic of Phenol and Lead Adsorption by Calcined Animal Waste

Phenol				Pb		
T (°C)	Δ*G* (kJ/mol)	Δ*H* (kJ/mol)	Δ*S* (J/mol·K)	Δ*G* (kJ/mol)	Δ*H* (kJ/mol)	Δ*S* (J/mol·K)
25	-1.04			-0.92		
30	-1.51			-1.25		
35	-2.12			-1.76		
40	-3.24	11.65	3.56	-2.06	21.72	5.83
45	-5.42			-2.64		
50	-6.32			-4.26		
60	-7.65			-5.03		

Desorption Studies

The desorption study results indicate a gradual decline in the efficiency of phenol and lead (Pb^{2+}) desorption over six cycles (Fig. 11), suggesting a reduction in the adsorbent's capacity in the course of cycles of regeneration. Initially, 72.5% of phenol and 77.2% of lead were desorbed, but by the fifth cycle, these values dropped to 52.5% and 56.1%, respectively. This decline suggests that some contaminants become more strongly bound to the adsorbent over time, likely due to structural changes, or pore blockage. The higher desorption efficiency for Pb^{2+} compared to phenol implies that lead ions may interact more weakly with the adsorbent than phenol, which likely forms stronger π-π interactions or hydrogen bonds.

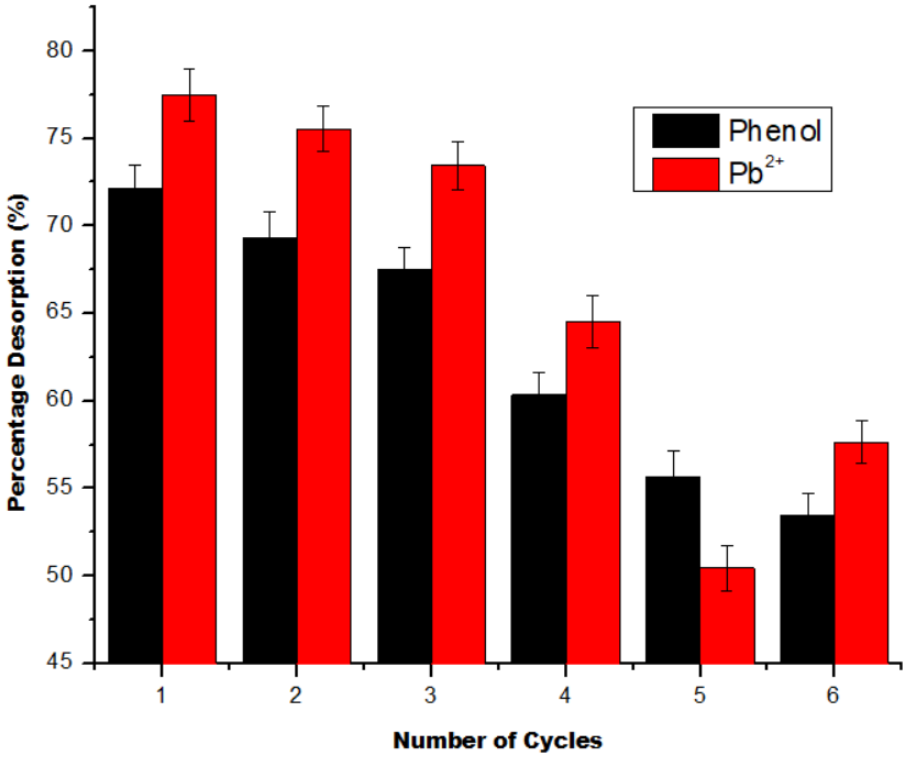

Fig. 11. Percentage desorption plots for phenol and lead adsorption by CAW

CONCLUSIONS

The potential of utilizing cellulose-based materials derived from animal waste (cow dung) for the adsorption of lead and phenol was investigated and the following are the highlights from the findings:

1. The adsorption efficiency was significantly impacted by initial pollutant concentration, pH, adsorbent dosage, temperature, and contact time.
2. Phenol adsorption more closely followed the pseudo-first-order kinetic model, while lead adsorption aligned with the pseudo-second-order model. Good fits were also achieved based on the interparticle diffusion model. The overall finding was that kinetics was mainly governed by rates of diffusion into a network of pores.
3. Langmuir isotherm analysis demonstrated the strong adsorption capacity of calcined cow dung-derived materials, favoring lead over phenol.
4. Adsorption of both phenol and lead was spontaneous and endothermic.
5. After the adsorption process, structural changes were confirmed from FT-IR and SEM analysis.

Conclusively, calcined animal waste-derived adsorbents present a promising, eco-friendly solution for removing lead and phenol from industrial wastewater, with high efficiency and practical applicability.

ACKNOWLEDGMENTS

The authors extend their appreciation for the financial support *via* the Researchers Supporting Project number (RSPD2025R754) from King Saud University, Riyadh, Saudi Arabia for funding this research.

REFERENCES CITED

Abdel-Ghani, N. T., El-Chaghaby, G. A., and Helal, F. S. (2015). "Individual and competitive adsorption of phenol and nickel onto multiwalled carbon nanotubes," *J. Adv. Res.* 6(3), 405-415. DOI: 10.1016/j.jare.2014.06.001

Ademoyegun, A. J., Babarinde, N. A. A., and Ofudje, E. A. (2022). "Sorption of Pb(II), Cd(II), and Zn(II) ions from aqueous solution using *Thaumatococcus danielli* leaves: Kinetic, isotherm, and thermodynamic studies," *Desalin. Water Treat.* 273, 162-171. DOI: 10.5004/dwt.2022.28877

Adeogun, A. I., Ofudje, E. A., Idowu, M. A., and Ahmed, S. A. (2012). "Biosorption of Cr(VI) ion from aqueous solution by maize husk: Isothermal, kinetic and thermodynamic study," *J. Chem. Soc. Pak.* 34(6), 1388-1396.

Akinhanmi, T. F., Ofudje , E. A., Adeogun, A. I., Aina, P., and Joseph, I. M. (2020). "Orange peel as low-cost adsorbent in the elimination of Cd(II) ion: Kinetics, isotherm, thermodynamic and optimization evaluations," *Bioresour. Bioprocess.* 7, article 34. DOI: 10.1186/s40643-020-00320-y

Akhtar, N., Syakir Ishak, M. I., Bhawani, S. A., and Umar, K. (2021). "Various natural and anthropogenic factors responsible for water quality degradation: A review," *Water* 13(19), article 2660. DOI: 10.3390/w13192660

Alexander, J. A., Zaini, M. A. A., Surajudeen, A., Aliyu, E. N. U., and Omeiza, A. U. (2018). "Insight into kinetics and thermodynamics properties of multicomponent lead(II), cadmium(II) and manganese(II) adsorption onto Dijah-Monkin bentonite clay," *Particul. Sci. Technol.* 36(5), 569-577. DOI: 10.1080/02726351.2016.1276499

Al-Ayed, O., El-Hasan, T., Amro, A., Matouq, M., and Kooli, F. (2022). "Treated oil shale ash and its capacity to remove Cd and Pb from aqueous solutions," *Oil Shale* 39(4), 308-324. DOI: 10.3176/oil.2022.4.05

Al-Ghouti, M. A., and Da'ana, D. A. (2020). "Guidelines for the use and interpretation of adsorption isotherm models: A review," *J. Hazard. Mater.* 393, article ID 122383. DOI: 10.1016/j.jhazmat.2020.122383

Aliyu, H. S., and Musa, A. (2021). "Lead: A concise review of its toxicity, mechanism and health effect," *GSC Biological and Pharmaceutical Sciences* 15, 055-062. DOI: 10.30574/gscbps.2021.15.1.0096

Alshomali, I., and Gulseven, O. (2020). "A note on SDG 6 – Clean water and sanitation for all," License CC BY-SA 4.0, Preprint, Available Online. DOI: 10.13140/RG.2.2.16461.38881

Babu, D. J., and Prasanna, P. K. Y. (2019). "Optimization of Cu (II) biosorption onto sea urchin test using response surface methodology and artificial neural networks," *Int. J. Environ. Sci. Technol*. 16, 1885-1896. DOI: 10.1007/s13762-018-1747-2

Briffa, J., Sinagra, E., and Blundell, R. (2020). "Heavy metal pollution in the environment and their toxicological effects on humans," *Heliyon* 6(9), article e04691. DOI: 10.1016/j.heliyon.2020.e04691

Chen, X., Yu, G., and Chen, Y. (2022). "Cow dung-based biochar materials prepared via mixed base and its application in the removal of organic pollutants," *Int. J. Mol. Sci.* 23(17), article 10094. DOI: 10.3390/ijms231710094

Collina, M. S, Senthil, K. V., Naveensubramaniam, V., Kanimozhi, V., Muhammad, A. S., Sibiya, S. R. G., Jogannagari, A., Rajan, C., Vladislav, L., Gabriel, I. T., *et al.* (2022). "Bioaccumulation of lead (Pb) and its effects on human: A review," *Journal of Hazardous Materials Advances* 7, article ID 100094. DOI: 10.1016/j.hazadv.2022.100094

Ettinger, A. S., Leonard, M. L., and Mason, J. (2019). "CDC's lead poisoning prevention program," *J Public Health Manag. Pract*. 25, S5-S12. DOI: 10.1097/phh.0000000000000868

Flouret, A., de Almeida, M. C., de Oliveira, T. F., and de Sá, F. P. (2018). "Advanced treatment of phenol by H_2O_2/UV/activated carbon coupling: Influence of homogeneous and heterogeneous phase," *Can. J. Chem. Eng*. 96(9), 1979-1985. DOI: 10.1002/cjce.23186

Freundlich, H. (1906). "Adsorption in solutions," *Phys. Chem.* 57, 384-410.

Ghahremani, A., Manteghian, M., and Kazemzadeh, H. (2021). "Removing lead from aqueous solution by activated carbon nanoparticle impregnated on lightweight expanded clay aggregate," *J. Environ. Chem. Eng*. 9(1), article ID 10447. DOI: 10.1016/j.jece.2020.104478

Günay, A., Arslankaya, E., and Tosun, İ. (2007). "Lead removal from aqueous solution by natural and pretreated clinoptilolite: Adsorption equilibrium and kinetics," *J. Hazard. Mater*. 146(1-2), 362-371. DOI: 10.1016/j.jhazmat.2006.12.034

Haitham, M. E.-B., Moushira, S., Reem, A. E.-G., Mahmoud, R. S., and Safnaz, M. T. (2022). "High adsorption capacity of phenol and methylene blue using activated carbon derived from lignocellulosic agriculture wastes," *Sci. Rep.* 12(1), article 5499. DOI: 10.1038/s41598-022-09475-4

Hamdy, A. A-G., Mohamed, S. A., Aya, H. M., Michael, B., Adrian, B.-P., Eder, C. L., Yasser, F. S., Mohamed, M., and Moaaz, K. S. (2023). "Utilization of red clay brick waste in the green preparation of an efficient porous nanocomposite for phenol adsorption: Characterization, experiments and statistical physics treatment," *Sustainable Chemistry and Pharmacy* 32, article ID 101027. DOI: 10.1016/j.scp.2023.101027

Howard, G., Calow, R., Macdonald, A., and Bartram, J. (2016). "Climate change and water and sanitation: Likely impacts and emerging trends for action," *Annu. Rev. Env. Resour.* 41(1), 253-276. DOI: 10.1146/annurev-environ-110615-085856

Hubbe, M. A., Azizian, S., and Douven, S. (2019). "Implications of apparent pseudo-second-order adsorption kinetics onto cellulosic materials. A review," *BioResources* 14(3), 7582-7626. DOI: 10.15376/biores.14.3.7582-7626

Issabayeva, G., Hang, S. Y., Wong, M. C., and Aroua, M. K. (2017). "A review on the adsorption of phenols from wastewater onto diverse groups of adsorbents," *Rev. Chem. Eng.* 34(6), 855-873. DOI: 10.1515/revce-2017-0007

Kanamarlapudi, S. L. R. K., Chintalpudi, V. K., and Muddada, S. (2018). "Application of biosorption for removal of heavy metals from wastewater," *Biosorption.* 69-115. DOI: 10.5772/intechopen.77315

Kinuthia, G. K., Ngure, V., Beti, D., Lugalia, R., Wangila, A., and Kamau, L. (2020). "Levels of heavy metals in wastewater and soil samples from open drainage channels in Nairobi, Kenya: Community health implication," *Sci. Rep.* 10(1), article 8434. DOI: 10.1038/s41598-020-65359-5

Kucherova, A. E., Romantsova, I. V., Burakov, A. E., Babkin, A. V., Neskoromnaya, E. A. and Krasnyansky, M. N. (2017). "Kinetic study on Pb (II) adsorption from aqueous solutions on carbon materials," *Nano Hybrids and Composites* 13, 334-340. DOI: 10.4028/www.scientific.net/NHC.13.334

Kshyanaprava, R., and Alok, P. D. (2023). "Lead pollution: Impact on environment and human health and approach for a sustainable solution," *Environmental Chemistry and Ecotoxicology* 5, 79-85. DOI: 10.1016/j.enceco.2023.02.001

Langmuir, I. (1918). "Adsorption of gases on plane surfaces of glass, mica and platinum," *J. Am. Chem. Soc.* 40(9), 1361-1403. DOI: 10.1021/ja02242a004

Li, Z., Chen, J., and Ge, Y. (2017). "Removal of lead ion and oil droplet from aqueous solution by lignin-grafted carbon nanotubes," *Chem. Eng. J.* 308, 809-817. DOI: 10.1016/j.cej.2016.09.126

Luo, Z., Gao, M., Yang, S., and Yang, Q. (2015). "Adsorption of phenols on reduced-charge montmorillonites modified by bispyridinium dibromides: Mechanism, kinetics and thermodynamics studies," *Coll. Surf. A- Phy. Eng. Asp.* 482, 222-230. DOI: 10.1016/j.colsurfa.2015.05.014

Makrigianni, V., Giannakas, A., Deligiannakis, Y., and Konstantinou, I. (2015). "Adsorption of phenol and methylene blue from aqueous solutions by pyrolytic tire char: Equilibrium and kinetic studies," *J. Environ. Chem. Eng.* 3(1), 574-582. DOI: 10.1016/j.jece.2015.01.006

Mishra, S., Yadav, S. S., Rawat, S., Singh, J., and Koduru, J. R. (2019). "Corn husk derived magnetized activated carbon for the removal of phenol and para-nitrophenol

from aqueous solution: Interaction mechanism, insights on adsorbent characteristics, and isothermal, kinetic and thermodynamic properties," *J. Environ. Manag.* 246, 362-373. DOI: 10.1016/j.jenvman.2019.06.013

Mlayah, A., Jellali, S., Azzaz, A. A., Jeguirim, M., Sellalmi, H., and Hamdi, N. (2021). "Investigations on lignite use for lead removal from aqueous solutions under static and dynamic conditions: Adsorption properties and mechanism exploration," *CR. Chim.* 24(S1), 7-22. DOI: 10.5802/CRCHIM.71

Mohammad, H. D., Sahar, A. S., Mojtaba, A., Mehdi, Q., and Mahmoud, S. (2023). "Removal of toxic lead from aqueous solution using a low-cost adsorbent," *Sci. Rep.* 13, article 3278. DOI: 10.1038/s41598-023-29674-x

Mustapha, S., Shuaib, D. T., Ndamitso, M. M., Etsuyankpa, M. B., Sumaila, A., Mohammed, U. M., and Nasirudeen, M. B. (2019). "Adsorption isotherm, kinetic and thermodynamic studies for the removal of Pb(II), Cd(II), Zn(II) and Cu(II) ions from aqueous solutions using *Albizia lebbeck* pods," *Appl. Water Sci.* 9, article 142. DOI: 10.1007/s13201-019-1021-x

Nabipour, H., Rohani, S., Batool, S. and Yusuff, A. S. (2023). "An overview of the use of water-stable metal-organic frameworks in the removal of cadmium ion," *J. Environ. Chem. Eng*. 11, article ID 109131. DOI: 10.1016/j.jece.2022.109131

Ofudje, E. A., Awotula, A. O., Alayande, S. O., Asogwa, K. K., and Olukanni, O. D. (2014). "Removal of lead (II) ions from aqueous solution by *Tricholoma terreum*: Kinetic studies," *Advances in Research* 2(2), 58-69.

Ofudje, E. A., Awotula, A. O., Hambate, G. V., Akinwunmi, F., Alayande, S. O., and Olukanni, O. D. (2017). "Acid activation of groundnut husk for copper adsorption: Kinetics and equilibrium studies," *Desalin. Water Treat.* 86, 240-251. DOI: 10.5004/dwt.2017.21339

Ofudje, E. A., Adeogun, A. I., Idowu, M. A., Kareem, S. O., and Ndukwe, N. A. (2020). "Simultaneous removals of cadmium (II) ions and reactive yellow 4 dye from aqueous solution by bone meal derived apatite: kinetics, equilibrium and thermodynamic evaluations," *J. Anal. Sci. Technol.* 11(1), article 7. DOI: 10.1186/s40543-020-0206-0

Ofudje, E. A., Sodiya, E. F., Ibadin, F. H., Ogundiran, A. A., Alayande, S. O., and Osideko, O. A. (2020). "Mechanism of Cu^{2+} and reactive yellow 145 dye adsorption onto eggshell waste as low-cost adsorbent," *Chem. Ecol.* 37(3), 268-289. DOI: 10.1080/02757540.2020.1855153

Ogundiran, A. A., Ofudje, E. A., Ogundiran, O. O., and Adewusi, A. M. (2022). "Cationic dye adsorptions by eggshell waste: Kinetics, isotherms and thermodynamics studies," *Desalin. Water Treat.* 280, 157-167. DOI: 10.5004/dwt.2022.29080

Puri, S., Sharma, S., Kumari, A., Sharma, M., Sharma, U., and Kumar, S. (2020). "Extraction of lignocellulosic constituents from cow dung: Preparation and characterisation of nanocellulose," *Biomass Conversion and Biorefinery* 13(4), 1-10. DOI: 10.1007/s13399-020-01119-9

Qasim, U., Osman, A. I., and Al-Muhtaseb, A. H. (2021). "Renewable cellulosic nanocomposites for food packaging to avoid fossil fuel plastic pollution: A review," *Environ. Chem. Lett.* 19, 613-641. DOI: 10.1007/s10311-020-01090-x

Salih, S. S., Kadhom, M., Shihab, M. A., and Tushar K. G. (2022). "Competitive adsorption of Pb(II) and Phenol onto modified chitosan/vermiculite adsorbents," *J. Polym. Environ.* 30(10), 4238-4251. DOI: 10.1007/s10924-022-02515-0

Samarghandi, M., Hadi, M., Moayedi, S., and Barjasteh, A. F. (2009). "Two-parameter isotherms of methyl orange sorption by pinecone derived activated carbon," *J. Environ. Health Sci. Eng*. 6, 285-294.

Samira, H. S., Hamadi, A., Rauf, F., Seyed, J. P., and Bahman, R. (2022). "Decontamination of Cd^{2+} and Pb^{2+} from aqueous solution using a magnetic nanocomposite of eggshell/starch/Fe_3O_4," *J. Water Proc. Eng*. 48, article ID 10291. DOI: 10.1016/j.jwpe.2022.102911

Sarker, N., and Fakhruddin, A. N. M. (2017). "Removal of phenol from aqueous solution using rice straw as adsorbent," *Appl. Water Sci*. 7(3), 1459-1465. DOI: 10.1007/s13201-015-0324-9

Shen, Y., Zhang, N., and Fu, Y. (2019). "Synthesis of high-performance hierarchically porous carbons from rice husk for sorption of phenol in the gas phase," *J. Environ. Manage.* 241, 53-58. DOI: 10.1016/j.jenvman.2019.04.012

Shi, S. L., Lv, J. P., Liu, Q., Nan, F. R., Jiao, X. Y., Feng, J., and Xie, S. L. (2018). "Application of phragmites australis to remove phenol from aqueous solutions by chemical activation in batch and fixed-bed columns," *Environ. Sci. Pollut. Res*. 25(24), 23917-23928. DOI: 10.1007/s11356-018-2457-5

Sobik-Szołtysek, J., Wystalska, K., Malinska, K., and Meers, E. (2021). "Influence of pyrolysis temperature on the heavy metal sorption capacity of biochar from poultry manure," *Mat.* 14, article 6566. Doi.org/10.3390/ma14216566

Strachowski, P., and Bystrzejewski, M. (2015). "Comparative studies of sorption of phenolic compounds onto carbon-encapsulated iron nanoparticles, carbon nanotubes and activated carbon," *Colloid. Surface. A.* 467, 113-123. DOI: 10.1016/j.colsurfa.2014.11.044

Thakur, V., Sharma, E., Guleria, A., Sangar, S., and Singh, K. (2020). "Modification and management of lignocellulosic waste as an ecofriendly biosorbent for the application of heavy metal ions sorption," *Mater. Today Proc*. 32, 608-619. DOI: 10.1016/j.matpr.2020.02.756

Thilakan, D., Patankar, J., Khadtare, S., Srushti, K., Nilesh, S. W., Jaya, L., Khalid, M. E-H., Saiful, I. M., Rabiul, I., Mohd, S. K., *et al.* (2022). "Plant-derived iron nanoparticles for removal of heavy metals," *Int. J. Chem. Eng.* 2022, article ID 151784. DOI: 10.1155/2022/151784

Upendra, R. D., Dilip, H. L., Anuj, K., Bidhan, P., and Mohd, U. (2023). "Adsorption of phenol using adsorbent derived from *Saccharum officinarum* biomass: Optimization, isotherms, kinetics, and thermodynamic study," *Sci. Rep.* 13(1), article 8356. DOI: 10.1038/s41598-023-42461-y

Vesali-Naseh, M., Vesali-Naseh, M. R. and Ameri, P. (2021). "Adsorption of Pb (II) ions from aqueous solutions using carbon nanotubes: A systematic review," *J. Cleaner Prod.* 291, article ID 125917. DOI: 10.1016/j.jclepro.2021.125917

Wang, J., and Zhang, W. (2021). "Evaluating the adsorption of Shanghai silty clay to Cd(II), Pb(II), As(V), and Cr(VI): Kinetic, equilibrium, and thermodynamic studies," *Environ. Monit. Assess.* 193, article 131. DOI: 10.1007/s10661-021-08904-7

Wang, T., Zheng, L., Liu, Y., Tang, W., Fang, T., and Xing, B. (2020). "A novel ternary magnetic Fe_3O_4/g-C_3N_4/Carbon layer composite for efficient removal of Cr(VI): A combined approach using both batch experiments and theoretical calculation," *Sci. Total Environ*. 730, article ID 138928. DOI: 10.1016/j.scitotenv.2020.138928

Wadekar, P. H., Khose, R. V., and Pethsangave, D. A. (2020). "Waste-derived heteroatom doped activated carbon/manganese dioxide trio-composite for

supercapacitor applications," *Energy Technol*. 8, article ID 1901402. DOI: 10.1002/ente.201901402

World Health Organization (WHO) (2019). "Lead poisoning and health," Available at: (https://www.who.int/news-room/fact-sheets/detail/lead-poisoning-and-health), Accessed 15 Oct 2024.

Yang, X., Li, L., Zhao, W., Wang, M., Yang, W., Tian, Y., Zheng, R., Deng, S., Mu, Y. and Zhu, X. (2023). "Characteristics and functional application of cellulose fibers extracted from cow dung wastes," *Materials* 16(2), article 648. DOI: 10.3390/ma16020648

Article submitted: December 18, 2024; Peer review completed: March 15, 2025; Revised version received: March 18, 2025; Second revised version received: March 21, 2025; Accepted: March 31, 2025; Published: April 9, 2025.
DOI: 10.15376/biores.20.2.3923-3952